The Environmental Fate of Marine Paints: Understanding Microplastic and Metal Release

Guadalupe Santos

Department of Chemical Engineering

McGill University, Montreal

December 2024

A thesis submitted to McGill University in partial fulfillment of the requirements of the degree of Master of Science in Chemical Engineering

Table of Contents

Abstract

Marine antifouling paints used on boats may release microplastics and metals to the aquatic environment when exposed to environmental stressors such as UV irradiation and freeze-thaw cycles. The fate of paint contaminants in the marine environment is not well understood as it is usually overlooked in microplastics studies. By using a variety of novel techniques, microplastics and metals released from weathered painted surfaces were characterized and quantified and the mechanisms of their release to the marine environment were determined. In this thesis, steel coupons painted with marine antifouling paint were submerged in water and exposed to three laboratory-controlled weathering conditions (i.e., UV irradiation (UV), freeze-thaw (FT), and UV-FT) and two temperature controls (i.e., cold temperature control (CC) and heat temperature control (HC)) for six weeks. Liquid samples were collected every two weeks and the generated paint particles and leachates were separated into two size fractions (>5 μm and <5 μm). Using optical photothermal infrared (O-PTIR) spectroscopy, inductively coupled plasma mass spectrometry (ICP-MS), single particle ICP-MS (SP-ICP-MS) and microscopic imaging, we quantified and characterized paint particles (i.e., microplastics) and metals released from antifouling paints.

Paint particles were detected in all weathering treatments and controls. The painted surfaces exposed to UV exhibited chemical changes likely due to oxidation, causing the degradation of the polymer matrix and release of microplastics. Freeze-thaw conditions generated the largest paint plastic particles through abrasion. When UV and freeze-thaw are combined (i.e., UV-FT), these conditions caused the release of the largest and highest number of paint particles (average mean 0.20 ± 0.10 mm and >67 ± 30 particles, respectively). Metal release from paints were quantified, where UV-FT conditions consistently released the most Cu and Zn over 42 days (220,000 ± 70,000 μg/g and 78,000 ± 20,000 μg/g, respectively). Cu was released mainly as paint

particles and was present at higher concentrations in weathering conditions involving abrasion (i.e., UV-FT and FT). In comparison, Zn was more likely to be leached in its dissolved form for the UV, HC and CC treatments. Higher temperatures were likely the reason for increased Zn leaching in UV and HC; however, the possible presence of calcium carbonate from the primer paint may have increased leaching for CC at cold temperatures. The different modes of release for the two metals may give insight into their uptake by organisms. Overall, our findings provide a deeper understanding of the mechanisms behind the release of paint contaminants into the environment, highlighting the environmental risks posed by the extensive use of marine antifouling paints and underscoring the need for effective pollution mitigation strategies.

Résumé

Les peintures antisalissures utilisées sur les bateaux peuvent libérer des microplastiques et des métaux dans l'environnement aquatique lorsqu'elles sont exposées à des facteurs de stress environnementaux tels que l'irradiation UV et les cycles de gel-dégel. Le sort des contaminants des peintures dans l'environnement marin n'est pas bien compris car il est généralement négligé dans les études sur les microplastiques. En utilisant une variété de nouvelles techniques, les microplastiques et les métaux libérés par les surfaces peintes altérées ont été caractérisés et quantifiés et les mécanismes de leur libération dans l'environnement marin ont été déterminés. Dans cette thèse, des coupons d'acier peints avec une peinture antisalissure marine ont été immergés dans l'eau et exposés à trois conditions d'altération contrôlées en laboratoire (irradiation UV (UV), gel-dégel (FT) et UV-FT) et à deux contrôles de température (contrôle de la température froide (CC) et contrôle de la température chaude (HC)) pendant six semaines. Des échantillons liquides ont été prélevés toutes les deux semaines et les particules de peinture et les lixiviats générés ont été séparés en deux fractions de taille (>5 μm et <5 μm). À l'aide de la spectroscopie infrarouge photothermique optique (O-PTIR), de la spectrométrie de masse à plasma à couplage inductif (ICP-MS), de la spectrométrie de masse à plasma inductif en mode particule unique (SP-ICP-MS), et de l'imagerie microscopique, nous avons quantifié et caractérisé les particules de peinture (c.-à-d. les microplastiques) et les métaux libérés par les peintures antisalissures.

Des particules de peinture ont été détectées dans tous les traitements contre les intempéries et dans les contrôles. Les surfaces peintes exposées aux UV présentaient des modifications chimiques probablement dues à l'oxydation, entraînant la dégradation de la matrice polymère et la libération de microplastiques. Les conditions de gel-dégel ont généré les plus grosses particules de plastique de peinture par abrasion. Lorsque les UV et la congélation-décongélation sont combinés

(c.-à-d. UV-FT), ces conditions entraînent la libération du plus grand et du plus grand nombre de particules de peinture (moyenne de 0,20 ± 0,10 mm et >67 ± 30 particules, respectivement). Les métaux libérés par les peintures ont été quantifiés, les conditions UV-FT ayant systématiquement libéré le plus de Cu et de Zn sur 42 jours (220 000 ± 70 000 µg/g et 78 000 ± 20 000 µg/g, respectivement). Le Cu a été libéré principalement sous forme de particules de peinture et était présent à des concentrations plus élevées dans les conditions d'altération impliquant une abrasion (c.-à-d. UV-FT et FT). En comparaison, le Zn était plus susceptible d'être lessivé sous sa forme dissoute pour les traitements UV, HC et CC. Des températures plus élevées sont probablement à l'origine de l'augmentation de la lixiviation du Zn dans les traitements UV et HC ; cependant, la présence possible de carbonate de calcium provenant de la peinture d'apprêt peut avoir augmenté la lixiviation dans le cas du traitement CC à des températures froides. Les différents modes de libération des deux métaux peuvent donner une idée de leur absorption par les organismes. Dans l'ensemble, nos résultats permettent de mieux comprendre les mécanismes à l'origine de la libération des contaminants des peintures dans l'environnement, en mettant en évidence les risques environnementaux posés par l'utilisation extensive des peintures antisalissures marines et en soulignant la nécessité de mettre en place des stratégies efficaces de réduction de la pollution.

Acknowledgments

This thesis would not have been possible without the support and assistance of the many individuals who contributed to my academic journey. I would first like to thank my supervisor Nathalie Tufenkji for her kindness and invaluable mentorship throughout my Masters. Her enthusiasm for microplastics research is always so inspiring. I am also extremely grateful for my co-supervisor, Kevin Wilkinson, for his helpful feedback on metals analysis and much appreciated guidance. I have learned so much from them both and it has made me into a better scientist. Thank you to my indispensable post-doctoral mentors: Laura Hernandez for providing the foundation of this project, and Georgina Kalogerakis for her support in driving both the project and me across the finish line. Thank you to Jun-Ray Macairan for answering all my questions related to O-PTIR and performing some very helpful O-PTIR analysis. I am thankful for Madjid Hadioui's invaluable expertise on the ICP-MS and SP-ICP-MS. Thank you to Houssame-Eddine Ahabchane for his knowledge on all things coding and SP-ICP-MS. Special thanks to Andrew Palucci and Izabela Junqueira Magalhaes, the two undergraduate students who have been so diligent in assisting me in the lab. Thank you to the members of the Biocolloids and Surfaces Laboratory and the Wilkinson lab for their amazing support and advice. Lastly, I'd like to give a big, heartfelt thank you to my parents and Ezra, who have given me constant encouragement and motivation when I needed it most.

I would like to acknowledge Jennifer Provencher from Environment and Climate Change Canada (ECCC) for supporting this project. Thank you to the following funding sources: the Fonds de recherche du Québec; McGill University through the Graduate Excellence Fellowships and Eugenie Ulmer Lamothe Entrance (EUL) Awards; the Advanced Technological Training network on the risk and remediation of Pollution in URban Environments (PURE CREATE); the Natural

Sciences and Engineering Research Council of Canada (NSERC); Centre De Recherche En Écotoxicologie Du Québec (EcotoQ); the Canada Foundation for Innovation; and the Canada Research Chairs program.

Contribution of the Authors

Laura M. Hernandez and Nathalie Tufenkji conceived the main concept. Guadalupe Santos, Laura M. Hernandez, Jennifer F. Provencher, Kevin J. Wilkinson, and Nathalie Tufenkji developed the experimental design. Guadalupe Santos and Georgina C. Kalogerakis prepared the materials and set up the six-week weathering experiments. Guadalupe Santos filtered, digested, diluted and analyzed paint samples for ICP-MS and SP-ICP-MS analysis; Madjid Hadioui gave valuable advice on the digestion procedure and analysis, as well as with troubleshooting the instruments. Guadalupe Santos acquired and analyzed spectra of the paint particles using O-PTIR spectroscopy; Jun-Ray Macairan analyzed the paint coupons using O-PTIR and provided guidance on the technique. Houssame-Eddine Ahabchane created the Python code for determining the Pearson correlation coefficient of the O-PTIR spectra of paint samples. Izabela Junqueira Megalhaes captured microscopy images of paint samples and Guadalupe Santos analyzed the obtained images with ImageJ. Andrew Palucci acquired the nanoparticle tracking analysis data of paint samples. Guadalupe Santos completed data management, statistical analysis and data visualization under the guidance of Georgina C. Kalogerakis, Laura M. Hernandez, Kevin J. Wilkinson and Nathalie Tufenkji. Guadalupe Santos wrote the thesis. Georgina C. Kalogerakis revised the manuscript along with Jun-Ray Macairan, Kevin J. Wilkinson and Nathalie Tufenkji.

Author List and Affiliations

G. Santos[1], G. C. Kalogerakis[1], J. R. Macairan[1], L. M. Hernandez[1], H. E. Ahabchane[2], J. F. Provencher[3], K. J. Wilkinson[2], N. Tufenkji[1]

[1] Department of Chemical Engineering, McGill University, Montreal, Quebec, Canada H3A 0C5

[2] Department of Chemistry, University of Montréal, Montreal, Quebec, Canada H2V 0B3

[3]Environment and Climate Change Canada, National Wildlife Research Centre, 1125 Colonel By Drive, Ottawa, Ontario, Canada K1A 0H3

List of Abbreviations

AAS	Atomic absorption spectroscopy
AF	Antifouling
AF-FFF	Asymmetric flow-field flow fractionation
ATR-FTIR	Attenuated total reflection Fourier transform infrared spectroscopy
CC	Cold control
DLS	Dynamic light scattering
EDX	Energy dispersive X-ray spectroscopy
F1	Fraction 1
F2	Fraction 2
F3	Fraction 3
FT	Freeze-thaw
FTIR	Fourier transform infrared spectroscopy
HC	Heat control
ICP-MS	Inductively coupled plasma mass spectrometry
ICP-OES	Inductively coupled plasma optical emission spectroscopy
MCE	Mixed cellulose ester
NP	Nanoparticle
NTA	Nanoparticle tracking analysis
O-PTIR	Optical photothermal infrared spectroscopy
PTFE	Polytetrafluoroethylene
py-GC-MS	Pyrolysis-gas chromatography-mass spectrometry

SEM	Scanning electron microscopy
SD	Standard deviation
SP-ICP-MS	Single particle inductively coupled plasma mass spectrometry
SP-ICP-TOF-MS	Single particle inductively coupled plasma time-of-flight mass spectrometry
TE	Transport efficiency
TEM	Transmission electron microscopy
UV	Ultraviolet
XRF	X-ray fluorescence spectroscopy

List of Figures

Appendix Figures

List of Tables

Appendix Tables

Chapter 1: Literature Review

1.1 Production, Use and Environmental Fate of Paints

The paints and coatings industry is a dominant and growing market. In 2019, the global demand for paint reached 52 million tonnes (Paruta et al., 2022). By 2022, the paints industry was valued at 202 billion US dollars (Pilcher, 2023). This growth is owed to the use of paint in various important sectors, such as the architectural, marine and automative industries.

Paint is a pigmented surface coating that is applied uniformly as a thin continuous layer to a surface. It is commonly used for decorative, protective, or specific technical purposes (OECD, 2014). Paints are composed of several ingredients: binders, pigments, dyes, extenders or fillers, and additives. The binder is the component that keeps all the paint ingredients in a cohesive matrix or material. Over 90% of binders used are synthetic and are composed of carbon-chain polymers such as alkyds, acrylics, polyurethane, and epoxies (Faber et al., 2021). Another ingredient of paint are metals, either existing as a pigment or as an additive, like biocides, catalysts, deodorants, flame retardants, and surfactants (Marrion & Guy, 2004). Outdoor painted surfaces such as boats, buildings and roofs are exposed to a range of environmental stressors (e.g. UV irradiation, wind, freeze-thaw, abrasion), resulting in their degradation (Turner, 2021). The degradation of the paint binder not only leads to the release of paint particles, i.e., microplastics, but also the release of other components, such as additives, embedded within the binder. The consequence, devastatingly, is paint pollution in the environment.

Paint particles have several sources and can reach environmental compartments in multiple ways. One source is the deterioration of roads and building coatings, as most roads are marked with paint, and buildings are coated with layers of protective paint. These two sources are examples

of how paint release products could end up in terrestrial compartments. Additionally, urban runoff can mobilize these particles to the marine environment (Turner et al., 2022). Horton et al. (2017) showed by Raman analysis that polymeric paint particles found in the Thames River basin matched sampled road marking paints. It was suspected that urban runoff carried the paint particles to the Thames basin. There are several direct sources of release of paint products to the marine environment; for instance, abandoned or grounded marine vessels and boat hull maintenance activities (Guimarães et al., 2022; Imhof et al., 2016; Ivar do Sul et al., 2014; Lagerström et al., 2017; Singh & Turner, 2009b; Soon et al., 2021; Ytreberg et al., 2016). These maintenance activities include cleaning boat hulls with dry dock abrasive, water blasting to remove organisms, as well as shot blasting, sanding, and stripping boat hulls of old paint (Singh & Turner, 2009b). Marine vessels are coated with antifouling paint, which is in some cases designed to be self-polishing, thus these paints shed their older outermost layer to expose a new layer underneath that contains higher levels of biocides. Friction between the hull and water is a source of antifouling paint particles (Faber et al., 2021). The abundance of paint particles in shipping routes may indicate antifouling paint as a major source of particle release (Dibke et al., 2021; Kwon et al., 2020; Mani et al., 2019). Indeed, Dibke et al. (2021) found that marine antifouling paint from marine vessels left polymeric particles, or “skid marks”, as they traveled through the sea.

1.2 Marine Paints

Paint is used in almost all surfaces of marine vessels, including the hull bottom, the waterline, topside structures, internal spaces, weather decks, and loose equipment. The two main paint types used in vessels are anticorrosive paints and antifouling paints. Anticorrosive paints are used to prevent corrosion formed on the vessel’s metallic components, whereas antifouling paints inhibit target organisms (e.g., algae, barnacles and biofilm) or biofouling, from attaching on the

hull bottom and at the waterline (Bighiu et al., 2017a). Preventing biofouling formation of the boat hull is important, as this can lead to an increase in fuel consumption from increased drag and even deterioration of the boat's structure (Bighiu et al., 2017a; Jin et al., 2022). To prevent biofouling of the boat hull, antifouling paint contains biocides such as copper oxides, zinc oxides, and other non-metallic biocides (Faber et al., 2021). In the past, metals such as lead and tin have been used as biocides; however, increased awareness about the toxicity of these metals have led to bans and strict regulations over the maximum admissible concentrations.

There are two types of antifouling paints: hard and soft (Akzonobel, 2017). Hard antifouling paint does not deteriorate quickly and generally contains a higher concentration of biocides, with leaching rates reducing over the service life of the product. Repainting is done every 2 to 3 years over the initial coating, forming a buildup of product that will need to be eventually removed (Faber et al., 2021). In contrast, soft antifouling paint is reapplied every year, since it degrades quickly over time via friction and dissolution. A subcategory of soft antifouling paints called self-polishing paints are designed to slough off the outer layer and antifouling agents at a controlled rate. Typically, a higher concentration of antifouling agents is revealed in the new, exposed layer. With all soft paints, particle release is inevitable.

1.3 Paint Pollution in the Environment

Paint particles are ubiquitous in the environment. Paint particles were found in oceans (Ivar do Sul et al., 2014), coastal waters (Chae et al., 2015; Kang et al., 2015; Kwon et al., 2020), sediments (Borges Ramirez et al., 2019; Horton et al., 2017; Jaouani et al., 2022; Mani et al., 2019; Mengatto & Nagai, 2022; Muller-Karanassos et al., 2019; Singh & Turner, 2009b), estuaries (Lima et al., 2014; Mengatto & Nagai, 2022), and lakes (Imhof et al., 2016; Jaouani et al., 2022) . Moreover, paint particles have been found inside a variety of organisms such as turtles (Caron et

al., 2018; Russell et al., 2011); fish (Abbasi et al., 2018; Cardozo et al., 2018; Neves et al., 2015; Ory et al., 2017); birds (Laist, 1997; Sileo & Fefer, 1987); crustaceans (Abbasi et al., 2018); cetaceans (Philipp et al., 2021); jellyfish (Iliff et al., 2020; Macali et al., 2018); and benthic organisms (Muller-Karanassos et al., 2019). Many studies suggest that paint particles may be one of the most significant contributors to microplastic pollution. For example, one study estimated that paint polyurethane particles were 30 times more abundant than plastics in the Antarctic Peninsula (Lacerda et al., 2019). Meanwhile, alkyd and epoxy plastics from paint may be the second most prevalent microplastic type in the North Atlantic (Turner et al., 2022).

The high additive content in paint gives rise to concern about the negative effects of paint particles on organisms. High concentrations of metal biocides have been observed to transfer to target organisms that grow on the surface of ship hulls, tracing it as a large source of metal pollution to the environment (Bighiu et al., 2017a). Additionally non-target organisms can also be affected. For example, cockles and ragworms exposed to environmentally relevant concentrations of antifouling paint particles caused high mortality (Muller-Karanassos et al., 2021). Earthworms were also found to be highly sensitive to antifouling paints, resulting in reduced mortality, body mass and reproductivity (Soroldoni et al., 2021). Toxicity of paints to other marine organisms were also confirmed in several studies (Bighiu et al., 2017b; Katranitsas et al., 2003; Soroldoni et al., 2020).

1.3.1 Microplastics and Nanoplastics Released From Paints

The paint binder makes up a large component of the paint (average of 37%) and is usually composed of a polymer that can produce secondary microplastics when weathered or abraded (Mengatto & Nagai, 2022; Paruta et al., 2022). These particles are distinguishable from other plastics as they are usually brittle, angular in shape, and layered (Turner et al., 2022). The scientific

literature usually ignores, misidentifies, or does not categorize paint particles as microplastics. Studies that have categorized paint particles found them to be composed of polyurethane (Lacerda et al., 2019), alkyd (Chae et al., 2015; Horton et al., 2017; Kang et al., 2015; Turner et al., 2022), epoxy (Dibke et al., 2021; Turner et al., 2022)), poly(acrylate/styrene) (Chae et al., 2015; Dibke et al., 2021), polyacrylate (Horton et al., 2017; Mani et al., 2019; Müller et al., 2022a) and chlorinated rubber (Dibke et al., 2021; Turner et al., 2022). Usually, studies do not specify the composition of the paint particles since researchers do not perform further confirmation with spectroscopic methods (Ivar do Sul et al., 2014; Jaouani et al., 2022; Kwon et al., 2020; Lima et al., 2014).

Paint particles detected in environmental samples can be as small as 1 μm to as large as 23 mm (Imhof et al., 2016; Song et al., 2014). The size range is within the microplastic definition, but does not breach the nanoplastic size range, since smaller particles are more difficult to identify using available analytical techniques. Several studies have highlighted that smaller particles seem to be the most abundant. Chae et al. (2015) found that most paint particles were in the 50 to 300 μm size range in their study, which was the smallest size fraction that they looked at. Another study by Mani et al. (2019) determined that most paint particles were present below 75 μm. Only a few studies have investigated nanoplastics in paints (Table 1). One study by Müller et al. (2022) found that nanoplastics sized 98 nm were present in one of the paints characterized. It was also observed that exposure to nanoplastics from the paint may be toxic to *Daphnia magna*, a model aquatic organism. Nanoplastics from house paint were also potentially released individually, or embedded in TiO_2 nanoparticles to create hybrid particles, as found by Fang et al. (2024).

Paint particles detected in marine environments have been shown to contain high concentrations of metals, such as Cu, Pb, Cr, Fe, Ti, and Zn (Gondikas et al., 2023; Turner et al., 2022). The presence of Cu, Sn, and Pb in the paint particles indicate the use of marine paints,

particularly antifouling paints. Studies suggest that marine paints may be the largest source of paint particles to aquatic environments, especially marine compartments. The particles may originate from shipping activities, as well as the maintenance and repair of ships and other similar structures (Chae et al., 2015; Ivar do Sul et al., 2014; Jaouani et al., 2022; Kwon et al., 2020; Mani et al., 2019; Mengatto & Nagai, 2022). For instance, one study by Chae et al. (2015) confirmed that paint particles found in the surface seawaters of Korea matched the paint collected from reference boats in shipyards.

It must be noted that the research vessel itself may also be a source of paint particles, which may lead to uncertainty in paint particle counts. For example, Lacerda et al. (2019) determined that some paint particles originated from the research vessel, as confirmed by Fourier-transform infrared (FTIR) spectroscopy analysis. Another study by Leistenschneider et al. (2021) attributed 45.5% of the paint particles to the research vessel when sampling in the Antarctic Sea. Therefore, care should be taken when assessing paint particles in microplastics studies.

1.3.2 Metal Nanoparticles Released From Paint

Engineered metal nanoparticles are materials added to paints to improve their properties, such as erosion, abrasion protection, UV light resistance, chemical resistance, and antifouling (Al-Kattan et al., 2015). Despite their extensive use, analytical data on the release of metal nanoparticles from paints, including their abundance, distribution, and persistence, is lacking, especially in environmentally relevant conditions. Laboratory-controlled weathering experiments have shown that metal nanoparticles leach from painted or stained surfaces into water (Table 1). By performing the leaching tests, these studies minimized external contamination from the environment, thus confirming that the nanoparticles came exclusively from the painted/stained surface. A study found that exposing painted panels to two years of UV weathering and

precipitation resulted in the leaching of 2.3% of the total SiO_2 particles (Al-Kattan et al., 2015). Meanwhile, Zuin et al. (2014) observed the leaching of TiO_2 (4 – 8 µg/L) and SiO_2 (73 mg/L) from three types of paints when subjected to UV-A irradiation and abrasion. Another study also also detected the release of TiO_2 (0.00048‰ of the total TiO_2 load on paint) and SiO_2 (0.38 – 0.62% of the total SiO_2 load on paint) when exposed to UV-A (Zhang et al., 2017). These studies show that different metals have different release rates. As shown in the studies mentioned, the loss of TiO_2 nanoparticles constituted an extremely small portion of the original concentration. In contrast, SiO_2 had a considerably more important release (Table 1).

Controlled weathering experiments do not accurately reflect what is found in environmental samples. Nevertheless, only a few studies have examined the effect of natural weathering on the release of metal nanoparticles from paints. These studies mainly looked at the influence of precipitation and flowing water in natural settings. For example, Kaegi et al. (2010) detected TiO_2 nanoparticles (a maximum of 600 µg/L) in runoff from one rainfall event which originated from naturally weathered painted facades. The authors also determined a strong release of Ag nanoparticles during early runoff events, observing a maximum Ag concentration of 145 µg/L. After a year, 30% of the original Ag load was released from the paint (Kaegi et al., 2010). Azimzada et al. (2020a) found that <0.001% of the TiO_2 load was lost from painted panels exposed to 10 weeks of natural weathering during the winter and summer. It was also found that a loss of 15% from total Ce from paints were observed over 12 weeks of winter exposure (Jreije et al., 2022). These studies demonstrate the pathways for loss of nanoparticles in natural settings, giving us more insight into what forms nanoparticles are found in the environment. Mentioned loss pathways include dissolution (as is the case for Ce), agglomeration (mainly for TiO_2) and transformation into less toxic chemical forms (as is proposed for Ag).

1.3.3 Metals Released From Paint

It is well documented that paints can leach metals, as some paints are designed for this purpose (e.g., antifouling paints). Environmental weathering can influence leaching rates of metals from paints. For instance, UV irradiation was shown to increase metal leaching by degrading the paint polymeric matrix (Simon et al., 2021). The study found that UV-exposed paints leached higher initial concentrations of Cu, Zn, Cd and Pb compared to non-exposed paints. High leaching can occur since UV irradiation can induce chemical and physical changes that alters the polymer structure of paint. Changes include a higher surface area and increased hydrophilicity because of the creation of hydrophilic functional groups in the paint matrix. Compounds like additives, fillers, and residual chemicals from paint production are thought to have high mobilities since they do not have chemical bonds with the paint matrix, resulting in their easier release into the environment (Simon et al., 2021).

Changing environmental parameters in weathering exposures can also affect the leaching rates of metals coming from paints. Parameters such as salinity, pH, temperature and presence of light have been tested (Holmes & Turner, 2009; Jessop & Turner, 2011; Singh & Turner, 2009b; Ytreberg et al., 2010). For example, Singh and Turner (2009) performed controlled weathering exposures where they observed increased leaching of Cu and Zn from antifouling paint with decreasing temperatures. The study attributed this phenomenon to complex reaction kinetics and the presence of dissolved calcium carbonate, which may be included as a component in the paint. They also found that increasing the salinity of the water increased the leaching rate of Cu and decreased the leaching rate of Zn (Singh & Turner, 2009b). Additionally, paint type and composition can influence leaching rates. A study found that due to higher hydrolysis rates, acrylic-based paints released higher concentrations of metallic biocides compared to epoxy- and resin-

based paints (Jalaie et al., 2023). Biocide-free paints were also found to release higher levels of Zn (4.4 – 8.2 μg/cm^2 day) compared to biocide-containing leisure boat paint and ship paints (3.0 μg/cm^2 day and 0.7 – 2.0 μg/cm^2 day, respectively) (Ytreberg et al., 2010). This is concerning since biocide-free paints are advertised as controlling biofouling via erosion and not by metal release. As such, biocide-free paints may be an important source of Zn to the marine environment.

The added metals in paints make them unique from plastics. One study utilized this distinction by considering particles containing more than 5% of Cu and Zn in their total inorganic composition as paint particles (Gondikas et al., 2023). Therefore, metal content may be a promising way of distinguishing paint particles from natural and anthropogenic particles.

1.4 Common Analytical Techniques for Analyzing Paints

1.4.1 Inductively Coupled Plasma Mass Spectrometry (ICP-MS)

Inductively coupled plasma mass spectrometry (ICP-MS) is a highly sensitive, analyte-specific technique used to analyze total metal content in environmental samples. For this analysis, an appropriate sample preparation must be performed. An aqua regia digestion is a typical approach to digesting paint particle samples (Turner et al., 2015). Alternatively, nitric acid can be used to digest and stabilize the metals in the medium (Wilschefski & Baxter, 2019).The liquid sample is then diluted and introduced into the instrument, where it is nebulized, producing an aerosol. An inductively coupled plasma, typically argon, atomizes and ionizes the ions in the aerosol, prior to their separation by a quadrupole mass analyzer that distinguishes particles according to their mass-to-charge ratio (Wilschefski & Baxter, 2019). Lastly, the metals present in the paint sample are then quantified based upon the number of ions reaching the detector and a calibration curve generated from an ionic standard. Numerous studies have used the technique to determine trace concentrations of metals in paints (Imhof et al., 2016; Kaegi et al., 2008; Ytreberg

et al., 2016). As such, it has been used as a standard comparison for analyzing metal content when using other novel techniques (Ytreberg et al., 2010). For instance, a study by (Ytreberg et al., 2017) compared metal concentrations measured with ICP-MS to a novel XRF technique. Both techniques exhibited a strong linear correlation with each other (Ytreberg et al., 2017).

1.4.2 Single Particle Inductively Coupled Plasma Mass Spectrometry (SP-ICP-MS)

Single particle ICP-MS (SP-ICP-MS) uses an ICP-MS as a basis to detect inorganic nanoparticles, particularly metal nanoparticles, at trace levels. This technique can determine particle size, particle mass, particle mass concentrations and dissolved metal concentrations with extremely low detection limits (Hadioui et al., 2019). Particle information is obtained by measuring particle events, or high-intensity signals, using extremely short measurement (dwell) times on the order of 25-100 µs (Goenaga-Infante & Bartczak, 2020). These peaks indicate the number of nanoparticles in the sample, while the intensity of the peaks denotes particle mass. Mass concentration can be calculated by summing all the masses of the particles and then dividing them by the sampled volume. The concentration of the dissolved fraction is determined from the constant signal (as a function of time), which can be distinguished from the detected spikes (or particles) in the sample. The high resolution and elemental specificity of SP-ICP-MS allows it to measure nanoparticles released from paint. This has been used to quantify several metal nanoparticles used extensively in paint such. For example, Azimzada et al. (2020) used SP-ICP-MS to determine the concentrations of TiO_2 particles released from naturally weathered painted panels. This technique has also been used to quantify Cu_2O nanoparticles from antifouling paints, CeO_2 nanoparticles from both paints and stains, and Ag from exterior façade paints (Adeleye et al., 2016).

1.4.3 Fourier Transform Infrared Spectroscopy (FTIR)

Fourier transform infrared (FTIR) spectroscopy is a valuable tool that can determine the chemical composition of organic material released from paints, such as polymers. This is done by exposing a sample to IR light, which is absorbed by various functional groups in the molecules. Functional groups absorb at specific frequencies (wavelengths) according to their molecular motions, which can provide valuable information on the chemical structure of the material. When comparing samples, changes in band frequencies and intensities can also indicate changes in the chemical structure. A popular mode of FTIR spectroscopy is Attenuated Total Reflection (ATR) since analysis can be quick and it does not require sample preparation. The method uses a crystal that comes in contact with the surface of the sample (Subramanian & Rodriguez-Saona, 2009). The crystal has a low refractive index, while the sample has a high refractive index. When an IR beam passes from the crystal to the sample, the light is reflected at a certain angle of incidence, called the total internal reflection. Some IR light, or the evanescent wave, escapes and is absorbed by the sample to produce a spectrum. FTIR has been used to identify paint particles that contain alkyds, epoxy resins, poly(acrylate/styrene), and polyurethane. Typically, FTIR and ATR-FTIR are used in conjunction with stereomicroscopy techniques to confirm the composition of a suspected paint particle (Chae et al., 2015; Jaouani et al., 2022; Kang et al., 2015; Kwon et al., 2020; Lacerda et al., 2019; Leistenschneider et al., 2021; Mani et al., 2019; Song et al., 2014; Turner et al., 2022).

1.4.4 Raman Spectroscopy

Raman spectroscopy is similar to FTIR in that it is also a vibrational spectroscopy technique. However, instead of measuring the light absorption, the technique measures molecular scattering. This in turn produces a vibrational spectrum representative of the chemical bonds in the sample. The vibrational frequencies provide a fingerprint of a particular compound based upon the

functional groups that are present (Araujo et al., 2018; Schlotter, 1989). The technique is favorably used for polymers and, by extension, microplastics. Owing to its high resolution, microplastics of the smaller size fraction can be analyzed using this technique. An extensive library needs to be built to match and detect paint particles in samples quickly, however, only a few studies have used Raman to identify paint particles in the environment (Horton et al., 2017; Imhof et al., 2016). This may be due to the difficulty in analyzing paints that have been weathered or the additive-rich content of paint particles.

1.4.5 Pyrolysis-Gas Chromatography-Mass Spectrometry (py-GC-MS)

Pyrolysis-gas chromatography-mass spectrometry, or py-GC-MS, uses an inert environment to thermally decompose samples (Käppler et al., 2015; Schlotter, 1989). The sample is fragmented into smaller molecules using pyrolysis, which are then called pyrolysis products. These products may be similar in structure to the original, larger molecule, or can be known by-products of the larger molecule. A GC column separates the pyrolysis products by their thermal lability mass and their affinity to the material of the column. After, a mass spectrometer measures the mass of each pyrolysis product from which the structure and chemical properties can be determined. Thermochemolysis can also be used as an added step for polar samples. This extra step hydrolyzes or methylates samples with polar functionalities so that GC-MS is a more suitable technique (Käppler et al., 2015). Only a fraction of compounds, i.e., the thermally labile ones, can be detected in GC. Py-GC-MS is an appropriate method for analyzing polymeric samples since they are non-volatile, which minimises losses during sample preparation. For example, a study by Dibke et al. (2021) has used this technique in analyzing the composition of ship “skid marks,” or plastic paint particles shed by a ship, with accurate polymer characterization.

1.4.6 Electron Microscopy Techniques (SEM, SEM-EDX, TEM, TEM-EDX)

Electron microscopy observes electron interactions with the material resulting in an image of the sample surface. The two main types of electron microscopy are scanning electron microscopy and transmission electron microscopy. In scanning electron microscopy (SEM), when an electron beam is directed at a metal-coated sample, electrons are reflected or knocked off and the deflected electrons are used to create an image of the sample surface. X-rays can also be emitted back because of the interaction between the sample and the electron beam. These X-rays will produce different energies depending on the elemental composition of the sample. Thus, via this technique, named energy dispersive X-ray spectroscopy (EDX), the elemental composition and concentration of the material can also be determined (Abd Mutalib et al., 2017). Scanning electron microscopy with energy dispersive X-ray spectroscopy (SEM-EDX) has been used extensively in analyzing paint particles (Kaegi et al., 2010; Lacerda et al., 2019). This technique is useful since polymeric paint particles are likely to have metals embedded within their matrix. It is also noted that nanoplastics can be examined using this technique (Sobhani et al., 2020), but only a few studies have used it to examine nanoplastics originating from paints (Müller et al., 2022b). For transmission electron microscopy (TEM), an image is produced from an electron beam passing through the sample, providing the structure and morphology of materials in the sample (C. Y. Tang & Yang, 2017). The images generated have an extremely high resolution, down to the picoscale. Like SEM, it has been used to examine metal nanoparticles in numerous paint-related studies (Kaegi et al., 2008, 2010; Zuin et al., 2014). Like SEM, EDX can also be combined with TEM (i.e., TEM-EDX).

1.4.7 X-Ray Fluorescence Spectroscopy (XRF)

X-ray Fluorescence, or XRF, is a quantitative and semi-quantitative technique that can be used to determine the concentrations of metals in a given sample area. It is a highly advantageous technique since it is non-destructive, cheap, and relatively quick (done in seconds or a few minutes). XRF analysis works by hitting the sample with X-rays, which then excites the atoms (Lagerström & Ytreberg, 2021). X-rays are emitted back by the atoms at specific orbital energies indicative of an element present in the sample. The instrument detects these energies, thus producing a spectrum that shows the concentrations of each specific element. Since the intensity of the detected XRF signal correlates with the concentration of the present element, calibration standards can be used for quantitative analysis. This technique cannot detect elements at a specific thickness, as X-rays cannot penetrate the sample. This is important since paints are multi-layered. One study found that the dry film thickness of an antifouling paint should remain below 40 microns to obtain accurate analyses (Ytreberg et al., 2017). Environmental samples can be analyzed with ease using XRF. This technique has been used to analyze metallic biocides in paints, especially antifouling boat paints that are known to have metal additives (Lagerström & Ytreberg, 2021; Ytreberg et al., 2016). This method is also used to confirm the source of paint particles (Leistenschneider et al., 2021; Zuin et al., 2014). For example, Turner et al. (2022) analyzed paint particles containing Cu and Sn, indicative of antifouling paint formulations used on boat hulls.

Table 1. Summary of literature examining the release of microplastics, nanoplastics and metals from paints.

Category of paint release product		Paint type	Sizes observed (average or range)	Concentration range/percentage composition released	Main analysis techniques*	Weathering conditions	References
Nanoplastics	Polyacrylate	Wall and ceiling paint	97 – 98 nm	Not specified	SEM-EDX, Raman, DLS, FTIR, AF-FFF	Dispersed in demineralized water	(Müller et al., 2022a)
	Suspected styrene or acrylic	House paint	<500 nm	Not specified	SEM-EDX, Raman	None	(Fang et al., 2024)
Microplastics	Unidentified thermoplastic	Road marking paints	1 – 4 mm	18.5 ± 4.2 – 66 ± 7.7 particles/100 g of sample	Optical microscopy, Raman	Natural: river	(Horton et al., 2017)
	Alkyds Poly(acrylate/styrene)	Industrial and marine based paints	<50 – 500 µm	171 ± 113 particles/L 24 ± 21 particles/L	FTIR	Natural: seacoast, Korea	(Song et al., 2014)
	Polyurethane	Contamination from the research vessel, continental sources and/or nautical equipment	0.3 – 23 mm	2805 particles out of filtered volume of 9127 m^3	FTIR, SEM	Natural: Antarctic peninsula	(Lacerda et al., 2019)
	Not specified	Marine based paints (boats, boat maintenance)	0.1 – 5 mm	Maximum approximately 900 particles/m^2	Optical microscopy	Natural: coastal sediments in an urban and natural drainage system	(Borges Ramirez et al., 2019)
	Alkyd Epoxy Chlorinated rubber	Marine based paints, building paints and road marking paints	Median: 180 µm	0.01 paint particles/m^3	XRF, ATR-FTIR	Natural: North Atlantic Ocean	(Turner et al., 2022)
	Not specified	Marine based paints	Most 1 – 3 mm	12.8% out of 398 microplastic particles	Optical microscopy	Natural: sediments from the Paranaguá Estuarine Complex	(Mengatto & Nagai, 2022)
	Acrylates, polyurethane, varnish (APV)	Marine based paints	<75 µm	Mean numerical proportion: 70 ± 19%	µFTIR,	Natural: Sediments from Rhine River	(Mani et al., 2019)

		(antifouling paint)			ATR-FTIR, Optical microscopy		
	Thermosetting polyester Epoxy resins	Marine based paints (boating and shipping activities)	Not specified	Not specified	FTIR	Natural: coastal waters of Plymouth	(Higgins & Turner, 2023)
	Alkyd resin (majority) Poly(acrylate/styrene)	Marine based paints	50 – >1000 µm	98.7% in surface microlayer 99.6% in surface seawater-hand net 60% in surface seawater -trawl net	FTIR	Natural: surface sea waters of Korean west coast	(Chae et al., 2015)Click or tap here to enter text.
	Not specified	Marine based paints	0.3 – 5 mm	0.03 – 0.65 paint particles/m^3	FTIR, Optical microscopy	Natural: surface waters of Korea	(Kwon et al., 2020)
	Not specified	Marine based paints	1 – 5 mm >5 mm	80% of total mesoparticles 32% of total macroplastics	ATR-FTIR, SEM-EDX	Natural: sediments in Tunisian coast	(Jaouani et al., 2022)
	Not specified	Marine based paints	Mean: <0.4 mm	12% of total plastic particles	Optical microscopy	Natural: plankton samples in Western Tropical Atlantic Ocean	(Ivar do Sul et al., 2014)
	Alkyd	Marine based paints (anticorrosive paints), contamination from the research vessel	<2 mm	0.94 to 232 particles/m^3	Optical microscopy, FTIR	Natural: southeastern coast of Korea	(Kang et al., 2015)
	Not specified	Marine based paints	<5 mm	29% of total particles	Optical microscopy	Natural: plankton samples in Western Tropical Atlantic Ocean	(Lima et al., 2014)
	Not specified	Marine based paints	4 µm – <10 mm	58 ± 58 particles/m^2	Raman	Natural: sediments from Lake Garda	(Imhof et al., 2016)
	Not assignable but suspected acrylates/ polyurethane/	Marine based paints, contamination from the research vessel	101 – 8932 µm	48% of total plastic particles	µXRF, ATR-FTIR	Natural: surface and subsurface water samples from Weddell sea	(Leistenschneider et al., 2021)

	varnish, polyester oxide						
	Poly(methyl methacrylate) Polyvinyl chloride Polycarbonate	Marine based paints	<1000 µm	Highest values: 53% (PMMA), 38% (PVC), 2% (PC)	py-GC-MS	Natural: from German Bight Waters	(Dibke et al., 2021)
	Not specified	Marine based paints (antifouling paints)	Not specified	0.01 – 3 mm	Optical microscopy, Raman, SEM-EDX	Natural: marinas on the Swedish coast	(Gondikas et al., 2023)
Metal nanoparticles	TiO_2 Ag SiO_2	Water-based paint	TiO_2: <10 nm Ag: 40 and 90 nm SiO_2: 12 nm	TiO_2: 4–8 µg/l Ag: Under detection limit (0.1 µg/l) SiO_2: 73 mg/l (1.8% of total SiO_2 in paint)	ICP-OES, TEM-EDX, XRF	UV irradiation (500 h, UV-A), abrasion (500 g load with 500 cycles/rotation)	(Zuin et al., 2014)
	SiO_2	Paint (with additive nSiO_2)	12 nm	0.065 mg/L (2.3% of the total nano-SiO_2 in panels)	ICP-OES, TEM-EDX	UV irradiation and precipitation (89 six-hour cycle, UV-A)	(Al-Kattan et al., 2015)
	TiO_2 Ag SiO_2	Paint (with nanoparticles)	Ti: 30 nm Ag: 50 nm Si: 10 nm	Ti: 0.00048‰ Ag: 0.025‰ to 0.055‰ Si: 0.38–0.62%	ICP-MS, DLS	Static water immersion test, UV irradiation (UV-A, 63 cycles of 8 h each), precipitation (500 h)	(Zhang et al., 2017)
	TiO_2	Behr Premium Plus Ultra Exterior Satin Enamel Ultra Pure white paint	20 – 60 nm	<0.001% of total nano-TiO_2 in paint	SP-ICP-MS	Natural weathering: 10 weeks winter, 7 weeks summer Lab: Room temperature, freezing (-10 C), freeze thaw (24 h freeze, 24 h thaw) for 42 days	(Azimzada et al., 2020a)
	TiO_2	Exterior façade paint	20 – 300 nm	Maximum 600 µg/L	ICP-MS, ICP-OES, TEM-EDX	Natural: Runoff (1 rain event)	(Kaegi et al., 2008)
	CeO_2	Behr Premium Plus ultra exterior satin enamel ultra-pure white paint, Stain (Syco)	17.5 nm (paint), 16.6 nm (stain)	15% (paint) and 35% (stain) of total NP-Ce in paint	SP-ICP-MS	Natural weathering: 11 weeks starting Oct and 12 weeks starting Jan	(Jreije et al., 2022)

	Ag	Exterior façade paint	Ag: <15 nm	30% of total NP-Ag in paint	ICP-MS, TEM-EDX	Natural: Runoff (65 runoff events, 372 days)	(Kaegi et al., 2010)
	TiO_2	Wall and ceiling paint	Up to 100 nm (in supernatant)	Not applicable	DLS, SEM-EDX, AF-FFF, Raman	Dispersed in Milli-Q water	(Müller et al., 2022a)
	Cu_2O	Antifouling paint	40 – 460 nm	0.21% of total Cu in paint (aluminum bars, 180 days) 1.76% of total Cu in paint (wood bars, 180 days)	SP-ICP-MS, DLS, SEM-EDX	Submerged panels with fluorescent light exposure and shaking (simulates natural waters) for 180 d	(Adeleye et al., 2016)
	TiO_2	Behr Premium Plus Ultra Exterior Satin Enamel Ultra-Pure White paint and SICO exterior semi-transparent wood stain	20 – >200 nm	10^{-4}% of total TiO_2 in paint 6% of total TiO_2 in wood stain	SP-ICP-MS, SP-ICP-TOF-MS	Natural weathering: 11 weeks starting Oct and 12 weeks starting Jan	(Azimzada et al., 2020b)
	TiO_2	Industrial paint	20 – 80 nm	0.007% of total nano-TiO_2	SEM-EDX, TEM	113 cycles, 6 h (3 hours of UV irradiation (UV-B), 0.5 h of irrigation and 2.5 h of drying)	(Al-Kattan et al., 2013)
	Cu	Marine based paints (antifouling paints)	45 – 100 nm	Maximum 1.2 x 10^7 particles/m^3	SP-ICP-MS	Natural: marinas on the Swedish coast	(Gondikas et al., 2023)
Total metals	Cu Zn	Boat paint fragments	Not available	Cu: ~16.0% of total Cu in dry paint (maximum) Zn: ~11.0% of total Zn in dry paint (maximum)	ICP-OES	Room temperature (19°C) or in refrigerator (4 °C) for 120 h; different salinities	(Singh & Turner, 2009b)
	Cu Zn	Antifouling paints (acrylic, epoxy and vinyl)	Not available	Cu: 70 µg/cm^2 day (acrylic, maximum) Zn: 64 µg/cm^2 day (acrylic, maximum)	AAS	Submerged in artificial sea water with wave-like conditions and at room temperature (23 °C)	(Jalaie et al., 2023)

	Cu Zn S Cd Pb Al	Marine antifouling paints	Not available	All percentages are maximums. Zn: 2.0% (paint mix), 0.1% (Alusafe) Cu: 0.2% (paint mix), 0.9% (Alusafe) S: 26.0% (paint mix), 5.0% (Alusafe) Cd: 4.5% (paint mix), 0.7% (Alusafe) Pb: 0.1% (paint mix) Al: 0.7% (Alusafe)	ATR-FTIR, ICP-OES	UV irradiation (UV-C) for 21 days, leaching in algae growth media for 168 h	(Simon et al., 2021)
	Cu Zn	Marine antifouling paints	Not available	Cu: 10.0 – 15.0% loss Zn: <8.0% loss	ICP-OES	Submerged in artificial sea water, with 12 h light-dark cycles using fluorescent tubes for 80 h	(Holmes & Turner, 2009)
	Cu Zn	Marine antifouling paints	Not available	Cu: 0.5% – 3.0% loss in aqueous phase Zn: 5.0 – 30.0% loss in aqueous phase	ICP-OES	Submerged in tap water (pH 7.3) or rainwater (pH 4.7) for 120 h	(Jessop & Turner, 2011)

*DLS: dynamic light scattering; AF-FFF: asymmetric flow-field flow fractionation; AAS: atomic absorption spectroscopy; ICP-OES: inductively coupled plasma optical emission spectroscopy; SP-ICP-TOF-MS: single particle inductively coupled plasma time-of-flight mass spectrometry

1.5 Knowledge Gaps

Many studies have explored the behaviour, fate, and impact of paints in the environment, yet this growing area of research remains an incomplete picture. Firstly, the release dynamics of most paint release products is still relatively unknown. Second, paint particles are difficult to distinguish from other anthropogenic particles such as microplastics. Therefore, assessing the quantitative contribution of paint particles as a proportion of the total microplastic distribution continues to be overlooked in microplastics literature. Lastly, techniques to quantify paint in environmental samples are limited and yet to be established.

(1) **Release dynamics:** There is a large body of literature for total metals released from paint, however, we note very few studies reporting the release dynamics for metal nanoparticles and microplastics. A variety of weathering exposures should be explored, as well as changes in the parameters of exposure (e.g. pH, water type, temperature). Studies should examine the kinetics and mechanisms of paint release products since it is crucial to furthering our understanding of their behaviour in the environment.

(2) **Identification of paint particles:** Many microplastics studies do not classify paint as a distinct category, owing to paints' similarity to other types of plastics. Typically, microplastics are categorized by the naked eye or by an optical microscope, and the classification methods are not standardized. As a result, paint particles may be ignored in the analysis (Torres & De-la-Torre, 2021). This highlights the importance of a more indisputable categorization that combines structure, brittleness, and polymer composition to distinguish paint particles from microplastics. For example, Gondikas et al. (2023) used the high Cu and Zn content characteristic of antifouling paints to be a method of distinguishing paint particles from other anthropogenic particles. Other studies have used

SEM-EDX, FTIR, and Raman for confirmation, but since sample isolation, preparation, and characterization are costly and time-consuming, they are usually not done for all samples collected in a study. In addition, the additive-rich content of paint makes it difficult to use familiar techniques such as FTIR and Raman that can be applied to microplastics. Paint pigments can interfere with these highly sensitive analyses, resulting in very little information obtained in the spectra. Moreover, the lack of a reference library creates a big challenge for identifying paint particles in the environment.

(3) **Analytical techniques:** Lastly, the limited capturing techniques and detection for paints may lead to imprecise, highly uncertain quantification in environmental samples. Many studies use the same techniques for paint as they do for microplastics. Paint has a higher density than microplastics, therefore most paints would inevitably be deposited in aquatic systems. If employing the same techniques used for microplastics, such as only looking at the surface waters in the aquatic environment, paints would be neglected in the analysis (Turner, 2021). There is also a possibility that paint particles found in environmental samples may be particles generated from the research vessel (Lacerda et al., 2019; Leistenschneider et al., 2021). This can be circumvented by using numerous blanks and controls to ensure reproducibility. If possible, research vessels designed to minimize paint contamination should be used in these studies.

1.6 Thesis Objectives

The main goal of this thesis was to characterize and quantify paint particles and metals released from submerged painted surfaces after exposure to weathering, which simulated different environmental stressors. The specific objectives were:

1) Determine the effect of weathering over time on surfaces painted with antifouling paint by simulating UV irradiation and freeze-thaw conditions relevant to cold climates.
2) Characterize and quantify products released from painted surfaces into an aqueous matrix, i.e., paint particles and/or metals, using a combination of novel techniques, such as O-PTIR and SP-ICP-MS. Specifically,
    a. changes (if any) to the paint binder were monitored,
    b. the sizes of paint particles released from the paint binder were determined,
    c. relevant metals in paint and their forms were identified, and
    d. particle and metal concentrations released from paints were determined.
3) Identify the possible mechanisms for the degradation of paint and its release products in a simulated aquatic environment.
4) Establish methodologies and techniques from which painted surfaces and their release products can be assessed in environmentally relevant conditions.

Chapter 2 will address the objectives and the overall goal of the project. This chapter will delve into the methodology (i.e., material preparation, weathering experiment setup, analysis of microplastics and metals released from paint), results and discussion of the experiments, as well as conclusions.

Chapter 2: Release of Microplastics and Metals From Weathered Marine Paints

Authors: G. Santos[1], G. C. Kalogerakis[1], J. R. Macairan[1], L. M. Rodriguez[1], Houssame-Eddine Ahabchane[2], J. F. Provencher[3], K. J. Wilkinson[2], N. Tufenkji[1]

[1]Department of Chemical Engineering, McGill University, Montreal, Quebec, Canada H3A 0C5

[2]Department of Chemistry, University of Montréal, Montreal, Quebec, Canada H2V 0B3

[3]Environment and Climate Change Canada, National Wildlife Research Centre, 1125 Colonel By Drive, Ottawa, Ontario, Canada K1A 0H3

2.1 Background

The marine industry heavily relies on paint. In 2022, the marine paint and coatings market was valued at $8.7 billion USD and the number is expected to continue growing every year (Gosselin, 2024). Marine paints are applied to the surfaces of structures and vessels (e.g., boats, ships, trawlers) that are regularly exposed to water to reduce the growth of sessile organisms or biofouling (Yebra et al., 2004). Since biofouling can affect vessel performance and fuel usage via increased drag (Adeleye et al., 2016), antifouling paint is applied to boat hulls to prevent the accumulation of organisms. Nonetheless, when marine paints are exposed to a range of environmental stressors (e.g., UV irradiation, wind, abrasion), the polymeric binder can degrade, generating paint particles that are largely microplastics. Furthermore, certain types of antifouling paints are designed to shed paint particles (i.e., self-polishing paints) (Lacerda et al., 2019; Yebra et al., 2004). As such, paint particles have been found in a variety of environmental matrices, including oceans, coastal waters, estuaries, lakes and sediments (Chae et al., 2015; Jaouani et al., 2022; J.-H. Kang et al., 2015; Mani et al., 2019; Mengatto & Nagai, 2022; Muller-Karanassos et al., 2019; Turner et al., 2022). For example, alkyd and epoxy plastics from paints were the second most abundant microplastic type found in the Atlantic Ocean (Turner et al., 2022).

Paint particles are unique from other microplastics because they contain high concentrations of metals. The metals are added as pigments or additives, such as biocides. In the

case of antifouling paints, copper (Cu), zinc (Zn) and lead (Pb) are often incorporated in the formulation as biocides. Subsequently, high levels of metal biocides have been found in marine waters and sediments close to high traffic areas and maintenance facilities (Biggs & D'Anna, 2012; Cunha et al., 2024; Hobbs et al., 2022). Paint particles generated from antifouling paint can detrimentally affect the function and behaviour of organisms, likely due to their high metal content. For example, high mortality was observed in cockles and ragworms when exposed to environmentally relevant concentrations of antifouling paint particles (Muller-Karanassos et al., 2021). Earthworms were also found to have increased mortality, reduced body mass and reduced reproductivity after exposure to antifouling paint particles (Soroldoni et al., 2021). For this reason, the use of certain metal biocides in antifouling paints, like organotin, have led to bans and strict regulations over the maximum admissible concentrations. On the other hand, metals such as Cu and Zn are largely unregulated and used as "less toxic" alternatives (Omae, 2003).

There exists a limited body of literature demonstrating the release of diverse contaminants (i.e., microplastics, nanoplastics, metals, and metallic nanoparticles) from different types of paints and the various analytical techniques detecting them. However, due to a lack of established analytical approaches to measure the released contaminants, our understanding of the fate of the paint-released products exposed to physical and chemical stressors in the environment remains incomplete. Simon et al. (2021) found that the chemical structure of the polymer binder in microplastics generated from marine antifouling paints was altered after exposure to UV-C irradiation. These changes included a higher surface area and increased hydrophilicity due to the generation of functional groups in the binder. Furthermore, the metals forms that are released from paints are also still largely uncharacterized. Although several papers have shown that metals are leached from these painted surfaces, only a few studies specify whether they exist as bulk

materials, nanoparticles or if they are released in dissolved forms. For example, Miller et al. (2020) found that Cu from an antifouling paint formulation was mainly released in its dissolved form, with the nanoparticulate Cu fraction constituting a maximum of 13.7% of the total Cu released over 120 days.

Other studies have examined some of the effects of environmental parameters in weathering exposures on leaching rates of metals coming from paints. For example, Singh & Turner (2009a) observed increased leaching with decreasing temperature for Cu and Zn from antifouling paint. They attributed the observed losses to complex reaction kinetics and the presence of dissolved calcium carbonate, which may be included as a component in the paint. They also found that increasing the salinity of the water increased the leaching rate of Cu and decreased the leaching rate of Zn. Additionally, paint type and composition can influence leaching rates. For example, acrylic-based paints were shown to release higher concentrations of metallic biocides compared to epoxy- and resin-based paints, a result that was attributed to higher hydrolysis rates (Jalaie et al., 2023). Biocide-free paints were also found to release higher levels of Zn (4.4 – 8.2 $\mu g/cm^2$ day) compared to biocide-containing leisure boat paint and ship paints (3.0 $\mu g/cm^2$ day and 0.7 – 2.0 $\mu g/cm^2$ day, respectively) (Ytreberg et al., 2010). This is concerning since biocide-free paints are advertised as controlling biofouling via erosion and not by metal release.

Information on the fate of paint-derived contaminants is important since it could reveal the underlying mechanisms of their release. Given their high toxicity, potential negative impact in natural environments, and their propensity to chemically change with time, it is necessary to evaluate the fate of paints under environmentally relevant conditions. Therefore, in this study, we aimed to: (i) quantify and characterize microplastics, metals, and metal nanoparticles released from painted surfaces; and (ii) examine the possible mechanisms for the release of microplastics and

metals when exposed to simulated UV irradiation and freeze-thaw conditions relevant to cold climates. By knowing the fate of paint-derived contaminants, we can develop a clearer picture as to what is being released and their behaviour in the environment.

2.2 Methods and Materials

2.2.1 Quality Assurance for Weathering Experiments and Chemical Analyses

Glassware was first cleaned three times with low foaming soap (Alconox® detergent, Millipore Sigma) and then rinsed three times with deionized water. Subsequently, the glassware was cleaned three times with acetone (C_3H_6O, ≥99.5%, Fisher Scientific) under a laminar flow hood and left to dry overnight. Sampling and other handling was also done under laminar flow.

2.2.2 Coupon Preparation and Paint Application

Test coupons (3 in. length × 2.5 in. width × 0.075 in. thick) were cut and deburred from a large low carbon steel plate (Catalog #6544K56, McMaster-Carr), following the guidelines adapted from ASTM D3623-78a.(ASTM International, 1998) The coupons were sanded using 80-grit sandpaper before being coated with four layers of epoxy primer (InterProtect 2000E, Interlux®) using a natural hog brush on both sides. Excess paint from each layer was removed with an applicator (Bird Film Applicator®, Inc, Washington, USA) in order to achieve a wet film thickness of 0.01 cm. After drying of the primer, two layers of antifouling (AF) paint (MicronCSC-CA, Interlux®) were applied using the same procedure mentioned previously. The final layer of paint was left to dry for at least 24 h before any water exposure, achieving a dry film coating with a thickness between 0.01 and 0.02 cm, in accordance with ASTM guidelines (ASTM International, 2020). Furthermore, the coupons were weighed before and after application of each type of paint to determine the weight of paint applied, achieving approximately 4.39 ± 0.27 g of primer and antifouling paint per coupon.

2.2.3 Experimental Setup and Experimental Matrix

Each coupon was placed in a pre-weighed 500 mL clean glass jar (Fisher Scientific) filled with 270 mL of demineralized water, which was then covered with a pre-cleaned glass Petri dish cover (Fisher Scientific). Demineralized water (resistivity >18.2 MΩ·cm, total organic carbon <5 ppb) used in weathering experiments were obtained from a Direct-Q™ 5 UV water purification system (Millipore Sigma).

Two types of coupons were tested for each weathering treatment: (i) coupons with only four layers of the primer and (ii) coupons with four layers of primer and two layers of AF paint (Figure 1). Procedural blanks, containing no coupon, were also included in the experiments to account for possible metal and plastic contamination (Figure 1). In the case of evaporation, the volumes of the jars were maintained by monitoring the weights, then adding the appropriate volume of demineralized water every two weeks during sampling.

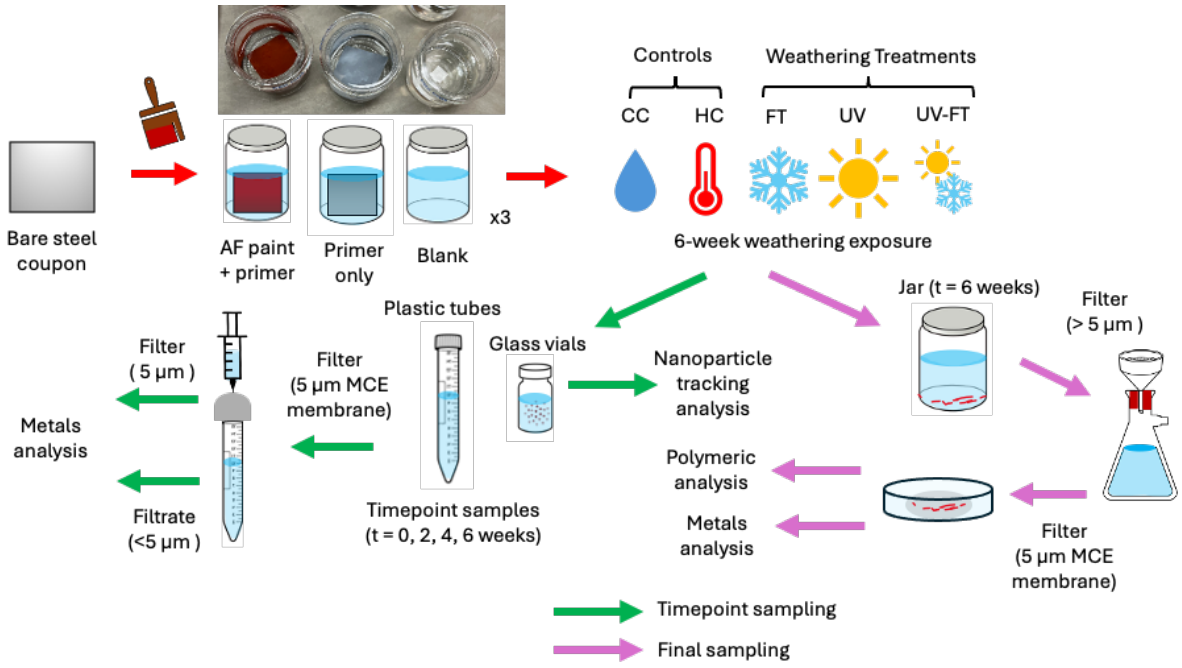

Figure 1. Overview of experimental setup, experimental matrix, sampling and chemical analysis.

Three weathering treatments were selected: (i) UV irradiation (UV), (ii) freeze-thaw (FT), (iii) combination freeze-thaw and UV (UV-FT). In addition, two controls were included: (i) a cold control (CC) and (ii) a heat control (HC) in order to provide a baseline of the release of paints due to temperature effects. The tested experimental conditions are summarized in Table 1. The UV treatment was carried out in a custom-made metal chamber equipped with reptile lamps (Arcadia 54w T5 D3+ 6% UVB 46", ReptilesRuS). For the UV treatment, the lamps were turned on and off every 24 h for 42 days, resulting in 21 UV cycles. During the UV exposure, the temperature in the chamber reached 30.3 ± 0.8 °C, while it was 22 ± 0.5 °C when the UV lights were turned off. For the FT treatment, coupons were placed in a freezer (-10.4 ± 3.8 °C, Samsung) for 24 h and then placed in the fridge for thawing (5.7 ± 2.1 °C, Samsung) for 24 h over 42 days (21 FT cycles). For UV-FT treatment, the coupons were exposed to UV light for 24 h and then placed in the freezer for 24 h, which also resulted in 21 UV-FT cycles. For CC, coupons were placed in the refrigerator (Samsung) for 42 days. For HC, samples were kept in an incubator (Multitron Pro, Infors HT) that was cycled (24 h) between 30 °C and 22 °C for 42 days. This cycling was done to mimic the UV treatment in order to only consider the effect of heat. For weathering treatments involving UV, UV radiation and photosynthetic flux were measured with the appropriate meters (i.e., Apogee MU-200 UV meter and Apogee MQ-100 Quantum Integral Sensor, respectively). For UV-FT experiments, samples were first acclimatized in the refrigerator for 30 to 60 min after every UV-FT cycle to reduce jar breakage. Triplicate samples were collected for each weathering condition.

Table 2. Experimental matrix for weathering treatments and controls.

Weathering treatment/ type of paint	**Cold control (CC)**	**Heat control (HC)**	**Freeze-thaw (FT)**	**UV**	**UV-FT**
Antifouling (AF) paint	AF paint, CC	AF paint, HC	AF paint, FT	AF paint, UV	AF paint, UV-FT
Primer paint	Primer paint, CC	Primer paint, HC	Primer paint, FT	Primer paint, UV	Primer paint, UV-FT
Procedural blank	Blank, CC	Blank, HC	Blank, FT	Blank, UV	Blank, UV-FT

2.2.4 Sampling of Weathered Paint Samples

Before the coupons were exposed to the various weathering treatments, 15 mL of the liquid paint sample from the jars were collected with a 5 mL pre-rinsed plastic pipette. Further aliquots (timepoint samples) were collected every 14 d to a maximum of 42 days during the weathering experiments. In that case, 15 mL of the water was sampled every 15 days in a sterile plastic tube (Corning Falcon) for metal analyses. Samples were refrigerated until analysis. At the end of the 42 days, the coupons were removed from the jar using a clean nitrile glove. The jars were then covered with PTFE-lined polypropylene caps (Fisher Scientific) and stored in the refrigerator until further analysis.

2.2.5 Size Separation of Paint Samples

The paint samples were divided into four size fractions for the analysis of particles and metals (Figure 2).

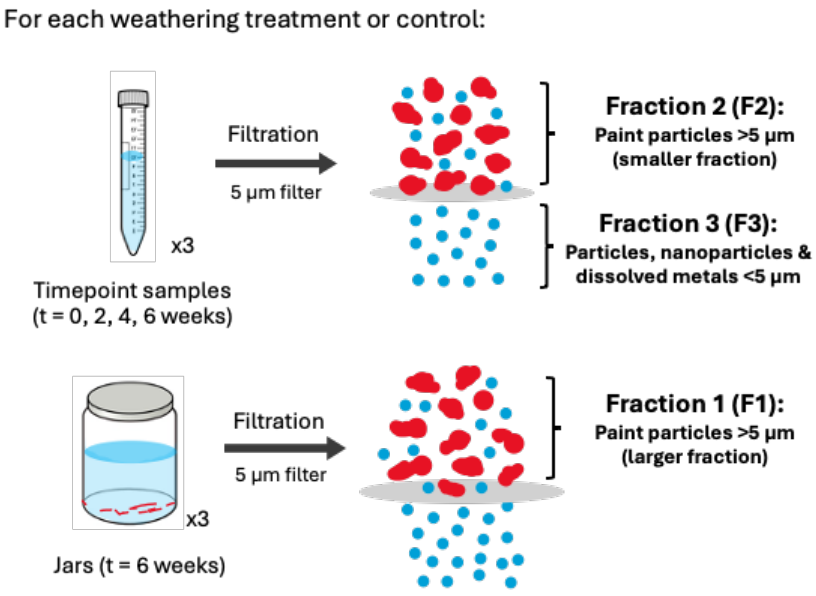

Figure 2. Size fractions of paint samples for timepoint samples (t = 0, 2, 4 and 6 weeks) and jar samples (6 weeks). Fraction 1 (F1), Fraction 2 (F2) and Fraction 3 (F3) were filtered with a 5 µm membrane. The number of replicates is indicated below the sample container.

Samples remaining in the jars at the end of the 42 d or 6-week weathering exposures, i.e., Fraction 1 (F1), were filtered using a glass vacuum filtration system (Sigma-Aldrich) under laminar flow. A mixed cellulose ester (MCE) membrane filter (diameter 47 mm, pore size 5 μm; MF-Millipore™) was placed in the filtration system and washed 3× with demineralized water. Then, the whole volume of the paint jar samples (~150 mL) was filtered. Using plastic tweezers, the filter from F1 was placed in a clean glass Petri dish labelled with a 100-square grid (Fisher Scientific) and then allowed to dry under laminar flow. Between samples, the filtration system was washed thoroughly with demineralized water and acetone to minimize any possible cross contamination between samples.

Timepoint samples were first sonicated for 30 min in a sonicator bath (Branson Ultrasonics, model CPX) and then filtered through a 5 μm filter that resulted in two fractions: (i) Fraction 2 (F2): retained paint particles >5 μm and (ii) Fraction 3 (F3): filtrate with paint particles <5 μm (Figure 2). Filtration was performed with a MCE membrane filter (25 mm diameter, pore size 5 μm; MF-Millipore™) that was placed in polypropylene filter holders (Cole-Parmer). The filter was first pre-rinsed with 12 mL of demineralized water and 6 mL of sample. Then, 5 to 9 mL of the sample was passed through the filter, and the filtrate (F3) was collected in 15 mL polypropylene Falcon tubes. Filters with retained particles were placed in 50 mL Falcon tubes using plastic tweezers (Fisher Scientific).

2.2.6 Chemical Analyses

Timepoint samples and the final suspension at the end of the experiment (final samples) were analyzed as described below. The exposed paint coupons were also analyzed, as shown below.

2.2.6.1 Nanoparticle Tracking Analysis (NTA) of Particles in Unfiltered Timepoint Samples

Samples collected in amber glass vials were sonicated in an ultrasonic bath (Branson Ultrasonics™) for 15 min. Approximately 1 mL of sample was analyzed with the NTA (NanosightPro, Malvern Panalytical Ltd). Five measurements were performed for each triplicate sample. Additionally, a procedural blank filled with demineralized water was sonicated and analyzed.

2.2.6.2 Detection of Cu_2O Nanoparticles Using SP-ICP-MS in F3

The timepoint sample filtrates (F3) were analyzed for metal nanoparticles using single particle inductively coupled plasma mass spectroscopy (SP-ICP-MS). Preparation of the samples were done similarly to Azimzada et al. (2020a). A multi-quadrupole ICP-MS (NexION® 5000 Series ICP-MS, PerkinElmer) was used to measure Cu-containing nanoparticles in F3. For size determinations, the composition and density (6.0 g/cm^3) were assumed to correspond to cuprous oxide (Cu_2O), since this is one of the main antifouling agents in the paint. Ionic standards (Inorganic Ventures IV-ICPMS-71A) were prepared for ^{63}Cu (0.05 –30 µg L^{-1}). Samples were analyzed for 50 sec using a dwell time of 100 µs. Transport efficiency (TE) was determined from 50 nm gold (Au) nanoparticles and ranged from 4.27% to 5.63%. Ionic silver (Ag) and Ag nanoparticles (approximately 60 ng/L) were used to validate the TE. Filtered samples were diluted 3–50 times, as required to ensure limited particle coincidence. Data were processed using the Syngistix software (PerkinElmer) and SPcal.(Lockwood, 2024) Organization of the large dataset was achieved using R and ChatGPT. Samples with <200 particle events (during 50 secs) were deemed to be below the limit of detection of the instrument and were discarded in the SP-ICP-MS analysis.

2.2.6.3 Imaging of Paint Particles >5 µm in F1

The counts and morphology of particles retained on the F1 filter of the final samples were determined using a stereomicroscope (Olympus, model SZX16). At least 30 representative pictures were taken for each sample, over an estimated area of 480 mm^2. The sizes of the particles were determined by using a ruler as a reference and by analyzing the images with ImageJ.

2.2.6.4 Analysis of Paint Coupons and Particles in F1 With mIRage®

The polymeric compositions of the weathered paint coupons and suspected paint particles in F1 were determined from optical photothermal infrared spectroscopy (O-PTIR) using the mIRage® IR microscope (Photothermal Spectroscopy Corp.). To minimize burning of the microplastics and to obtain a high intensity signal, an avalanche photodiode detector was utilized in the analysis. Three random fields of view where suspected particles and agglomerates could be seen were selected. In each field of view, at least nine IR spectra from random individual particles were acquired (2998 – 2688 cm^{-1} and 1798 – 940 cm^{-1}).

A Pearson correlation coefficient was used to compare the treatments and controls against the reference, virgin antifouling paint (Abd Rashid et al., 2023; Primpke et al., 2020; Simon et al., 2021). This coefficient measures the strength and direction of a linear correlation between two different sets of data (Abd Rashid et al., 2023; Primpke et al., 2020; Simon et al., 2021). It can be between -1 and 1 for a perfect negative and perfect positive correlation, respectively, with a value of 0 indicating no relationship.

2.2.6.5 Metals Analyses of F1, F2, and F3

All three fractions (F1, F2 and F3) were analyzed for total metal concentrations of ^{63}Cu and ^{66}Zn using a multi-quadrupole ICP-MS (NexION® 5000 Series ICP-MS, PerkinElmer). For F1 and F2, filters were placed in 50 mL polypropylene Falcon tubes and then digested with aqua

regia. For F3, filtrate samples were acidified with 2% v/v ultrapure nitric acid for 24 to 48 h. Procedural blanks were also prepared, digested and analyzed. F1 and F2 samples were diluted to 4% v/v acid before analysis, with additional dilutions performed, if required. Calibration standards of IV-ICPMS-71A (Inorganic Ventures) were prepared, ranging from 0.05 – 30.00 ppb in a 2% nitric acid. Standards (SCP Science Quality Ctrl. Std. 4 and High Purity Standard 27 Component ICP Standard) were used to ensure quality control. Concentrations from the procedural blanks were subtracted from the original calculated concentrations to account for contamination.

2.3 Results and Discussion

2.3.1 Confirmation of the Identity of Paint Particles With O-PTIR

The paint that was studied is self-polishing, i.e., the outer layer of the paint is designed to slough off upon exposure to water, and as such, paint particles were detected in all samples. For the fraction F1 (>5 μm after 6 weeks of weathering), paint particles that were released from the painted coupons were identified using O-PTIR. In all weathering treatments and controls, major peaks in their spectra matched with characteristic peaks in the spectrum of the virgin AF paint, i.e., the reference paint (Figure 3A).

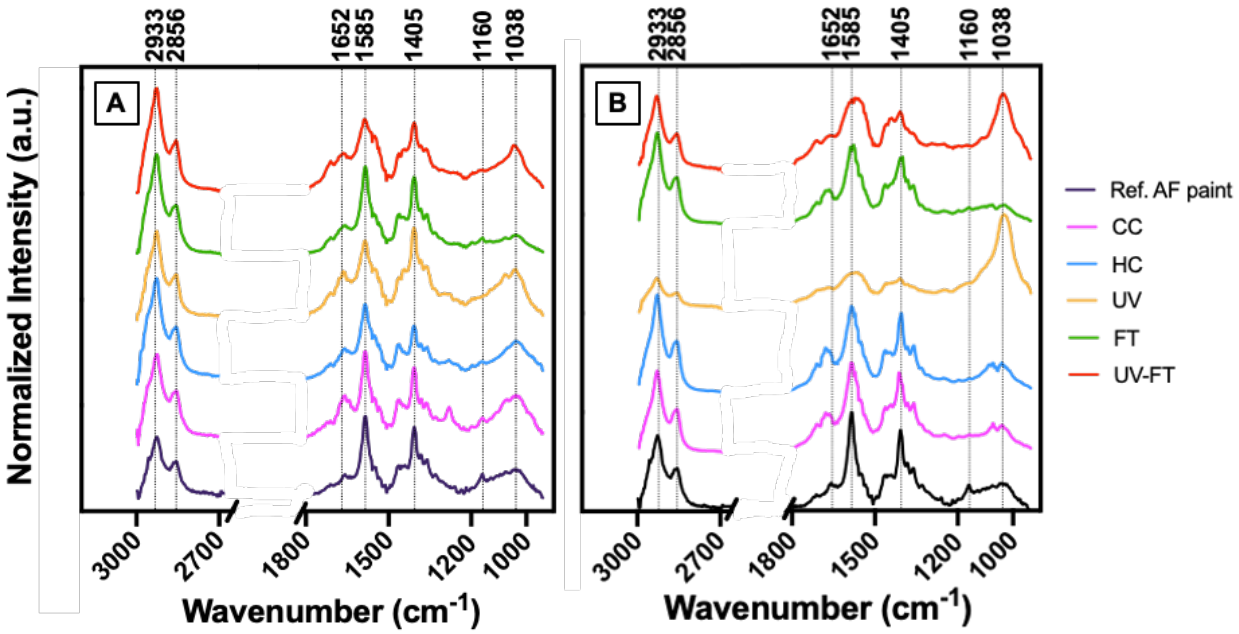

Figure 3. Averaged normalized spectra of (A) paint particles collected from the exposure water after 6 weeks (i.e. F1) and (B) paint coupons following their exposure after 6 weeks to one of five weathering treatments or controls: (i) CC = cold control; (ii) HC = heat control; (iii) UV = UV irradiation; (iv) FT = freeze-thaw; and UV-FT = UV and FT combination. All spectra can be compared to the average normalized spectra of the virgin reference AF paint, denoted as Ref. AF paint. Common wavenumbers shared among all spectra are labelled on the upper y-axis (over the range 3000 cm^{-1} to 940 cm^{-1}).

In assigning peaks to different components of the paint, most could be attributed to the binder, or polymeric component (Table 2). The safety data sheet of the AF paint did not indicate what type of polymer was used for the binder (Table A1), and matching the spectra with a database proved difficult. Nonetheless, the spectra were found to be similar to those observed for a nautical paint studied by Simon et al. (2021). The paint in their study was also a self-polishing antifouling paint, using zinc oxide (ZnO) and Cu_2O as its metal biocides. In that case, the binder that was used was mainly rosin, a naturally occurring polymer, which can be categorized as a microplastic if chemically altered for a given application, such as paint (Simon et al., 2021). Indeed, the AF paint used in this study contained metal-carboxylic acid groups (1585 and 1485 cm^{-1}) that are indicative

of a rosin-based binder (Table 2). Furthermore, the AF paint studied here lacked the ester group C=O stretch at 1726 cm^{-1} and the carbonyl stretch at 1733 cm^{-1}, which would implicate acrylic or alkyd-based paints, respectively (Germinario et al., 2016; Hayes et al., 2014; Simon et al., 2021).

Table 3. Peak assignments (cm^{-1}) for spectra acquired with O-PTIR for weathered and virgin AF paint particles. Assignments are based on Hayes et al. (2014), Simon et al. (2021) and van der Weerd et al. (2005).

Wavenumber (cm^{-1})	Functional group	Class	Origin
2933	Methylene asymmetric C–H stretch	Alkane	Binder
2856	Methyl symmetric C–H stretch	Alkane	Binder
1652	C=C stretch	Alkene	Binder
1585	Metal carboxylate asymmetric COO stretch	Carboxylic acid	Binder
1405	Metal carboxylate, symmetric COO stretch	Carboxylic acid	Binder
1160	CO	Carboxylic acid	Binder
1038	Si-OR	Silicate	Pigment

Based upon the strength of the Pearson correlation coefficient, no obvious spectral changes were found when comparing spectra from the weathered paint microparticles to the virgin AF paint (Figure 3A). High positive correlations were calculated for all weathering treatments and controls (n = 27 spectra for each treatment) when compared to the reference AF paint (n = 9 spectra): 0.81 ± 0.21 for CC, 0.92 ± 0.02 for HC, 0.91 ± 0.03 for UV, 0.88 ± 0.03 for FT, and 0.95 ± 0.02 for UV-FT (Figure A1, text A1). The peak at 1282 cm^{-1} was only present for one replicate of CC and is also found in the spectra of the MCE membrane filter (Figure A2). Since some of the particles analyzed in CC were very small (Figure A3), the laser of the O-PTIR instrument may have detected the MCE membrane filter on which the paint particles rested.

2.3.2 UV Induced Chemical Changes in the Painted Coupons

On the other hand, the physical appearance of the weathered painted coupons was clearly modified after six weeks of exposure as compared to the two control coupons (HC and C; Figures

A4 and A5). Furthermore, based upon the O-PTIR spectra (Figure 3B), the paint on the weathered coupons exhibited some important chemical changes when compared to the virgin AF paint, especially for the UV and UV-FT treatments. When compared to the reference paint on the coupons, the Pearson correlation coefficients were as follows: 0.91 ± 0.03 for CC, 0.91 ± 0.02 for HC, 0.28 ± 0.18 for UV, 0.92 ± 0.01 for FT, and 0.69 ± 0.25 for UV-FT (Figure A6).

Images of the coupons obtained from O-PTIR confirmed that treatments exposed to UV irradiation had smoother surfaces compared to the controls and FT treatment (Figure A5). Chemical changes, subsequent to the UV and UV-FT exposures, were confirmed by the broadening of several of the characteristic peaks (Figure 3B). UV radiation is known to accelerate chemical reactions in materials and cleave chemical bonds (primarily C-H and C-O) (González-Cabrera et al., 2021). UV can also promote oxidation, inducing the formation of hydroxyl groups in the unsaturated groups of paint binders (Azémard et al., 2014; Simon et al., 2021). Indeed, the peaks at 1652, 1595, and 1405 cm^{-1}, indicative of alkene and metal carboxylate groups, lost their sharpness in the AF paint coupons exposed to UV and UV-FT. This observed broadening is consistent with the formation of hydroxyls on the unsaturated groups, resulting in the degradation of the polymer material. Methylene groups (2933 and 2856 cm^{-1}) in the UV and UV-FT treatments were also found to have broadened, which can be attributed to the loss of volatile organic compounds and degradation products in the rosin binder (Azémard et al., 2014). Noticeably, the peak at 1038 cm^{-1}, indicating a silicate functional group, increased for UV and UV-FT in comparison to the virgin AF paint and other weathering conditions. Silicates are UV stable, therefore the signal should also remain constant (Jost et al., 2016). However, due to normalization, the broadening of peaks for the other functional groups (wavelengths >1200 cm^{-1}) may have led to a false impression that higher amounts of silicate were found for UV and UV-FT.

Compared to the paint coupons, the paint particles did not exhibit noticeable chemical changes. The generated paint particles may have been shielded from UV by the coupon, reducing the effect of UV. Additionally, water submersion has been shown to hinder the degradation effect of UV on polyethylene films (Kalogerakis et al., 2017). In our experiments, the larger paint particles settled to the bottom. Therefore, some of the UV irradiation could have been absorbed by the water, limiting chemical changes in the paint particles. Indeed, when comparing the weathered paint particles to the coupons, the UV-only exposed coupon had the lowest similarity to all paint particles, regardless of the type of treatment (Figure A7, Table A3). Somewhat surprisingly, the UV-FT exposed coupon had a higher similarity than the UV-only treatment to the weathered paint particles, despite having the same UV exposure time (Table A3). These results suggest that the FT exposure may have a hand in reducing the oxidizing effect of UV irradiation. Overall, the O-PTIR spectra of the UV-exposed paint coupons gives evidence of the weakening of the polymer structure via UV-induced oxidation that can result in the generation of paint microparticles (Y. Kang et al., 2025; Simon et al., 2021). The results also demonstrate that in natural waters, determining the source of paint-derived microplastics, especially those arising from UV exposure, will prove difficult.

2.3.3 Detection and Generation of Paint Particles >5 µm in F1

Paint particles were detected in all F1 fractions that were collected after six weeks of weathering, including the controls (Figure 4). The numbers and sizes of the particles were determined for each treatment, except for the UV-FT treatment (Table A4). In that case, it was not possible to accurately determine particle counts since the 5 µm filter was fully saturated with microplastics, confirming that the UV-FT condition generated the most particles, followed by FT. An average of 67 ± 30 particles/mL were detected in the FT treatment (Table A4). Therefore, the

number of particles generated in the UV-FT treatment was much higher than the FT treatment. For the UV treatment, high counts of microplastics were detected (14 ± 10 particles/mL) compared to the HC and CC controls (6 ± 6 and 2 ± 3 particles/mL, respectively).

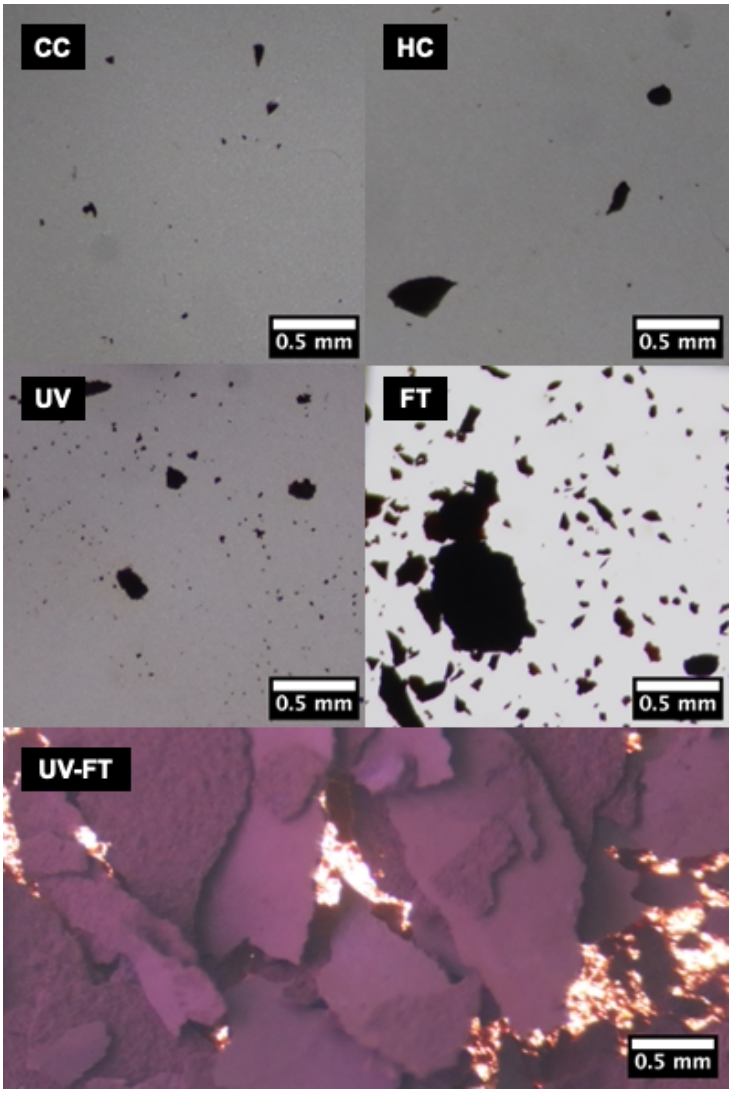

Figure 4. Optical microscope images of paint particles released from controls (i.e., CC = cold control, HC = heat control) and weathering treatments (i.e., UV = UV irradiation, FT = freeze-thaw, and UV-FT = UV and FT combination).

The lowest number of particles detected was in CC, followed by HC. Though both controls did not experience any weathering per se, the higher temperatures for the HC (cycling between

30.1 ± 0.2°C and 22.8 ± 0.4 °C) may have generated more particles than the exposure to a constant, cold temperature (5.7 ± 2.1 °C). Plastics tend to degrade when exposed to higher temperatures. For example, one study found that exposure of polyvinyl chloride to 50 °C and 100 °C resulted in a "melting" of the plastic surface, making it susceptible to degradation (Tang et al., 2018). Another study with more environmentally relevant temperatures found that temperatures in the summer months induced degradation via thermo-oxidation in polyethylene films, producing microplastics (Kalogerakis et al., 2017). Though many studies use much higher temperatures than what was tested in the current experiments, our results indicate that paint-derived microplastics can be generated more quickly even with only a ~25 °C difference between the temperature controls.

Larger paint particles were more prevalent in conditions involving FT cycles (Figure 5). The largest paint particles were detected in the UV-FT treatment as compared to all other treatments and controls (maximum size 4.8 ± 0.1 mm and mean size 0.20 ± 0.10, Table A4). This was followed by FT (maximum size in the replicates 3.3 ± 1.0 mm; mean size in the replicates 0.07 ± 0.02; Table A4). Measured paint particles from the rest of the treatments and controls did not exceed 1.1 ± 0.7 mm (maximum particle size for HC). Freeze-thaw cycles can abrade a material via ice abrasion by: (i) creating cracks via tensile stress, which can be exacerbated by seeping of water into the cracks that can be frozen again, (ii) releasing fragments that can be dragged onto the original material's surface by the ice, and (iii) hydraulic pressure encouraging fracturing within surface defects of the material (Jacobsen et al., 2015). For standing painted marine structures in the tidal zone, such as concrete structures, FT cycles can happen frequently (Thomas, 2016). However, many boats are stored during the winter, at a height at which FT cycles happen. As such, the generation and release of paint particles can be delayed. Boats stored in slipways and hard standings can generate paint particles that can then be deposited onto the ground (Turner et al.,

2015). Spring surface runoff can potentially transport these paint particles back into the aquatic environment (Turner, 2021).

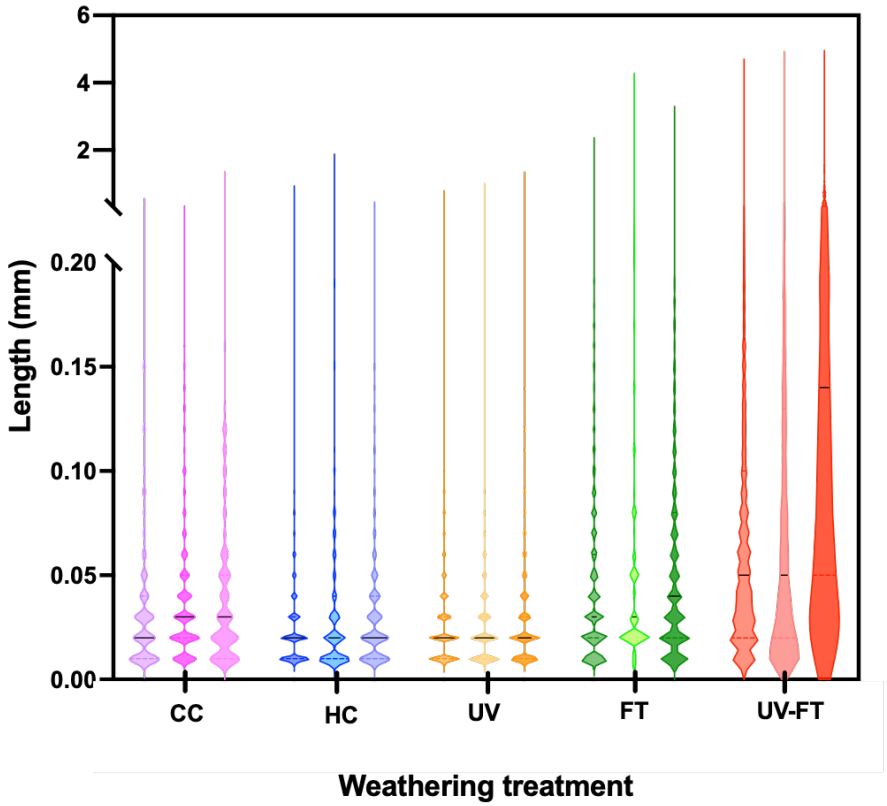

Figure 5. Violin plots of the size distributions of paint particles released from the temperature controls and weathering treatments (CC = cold control, HC = heat control, UV = UV irradiation, FT = freeze-thaw, and UV-FT = UV and FT combination). The size distribution for each individual triplicate sample is shown. Dotted lines indicate the quartiles, and the solid black lines indicate the median.

2.3.3 Temporal Release of Copper and Zinc From Paint

Given that Cu_2O and ZnO are the biocidal ingredients for the paint used in this study, Cu and Zn were analyzed by ICP-MS (Table A1). Cu and Zn release into the F2 (paint microparticles) and F3 (5 µm filtrate) fractions are shown in Figure 6. The UV-FT treatment consistently released the most Cu and Zn from the paints. At the final timepoint (6 weeks), 17.0 ± 3.0 mg/g of Cu and 6.7 ± 2.0 mg/g of Zn were released during the UV-FT treatment (Figures 6A and B). These

concentrations are in line with a previous study that found extremely high concentrations of 400 mg/g Cu and 250 mg/g of Zn collected from a boat maintenance facility and attributed to paint particles (Turner, 2010).

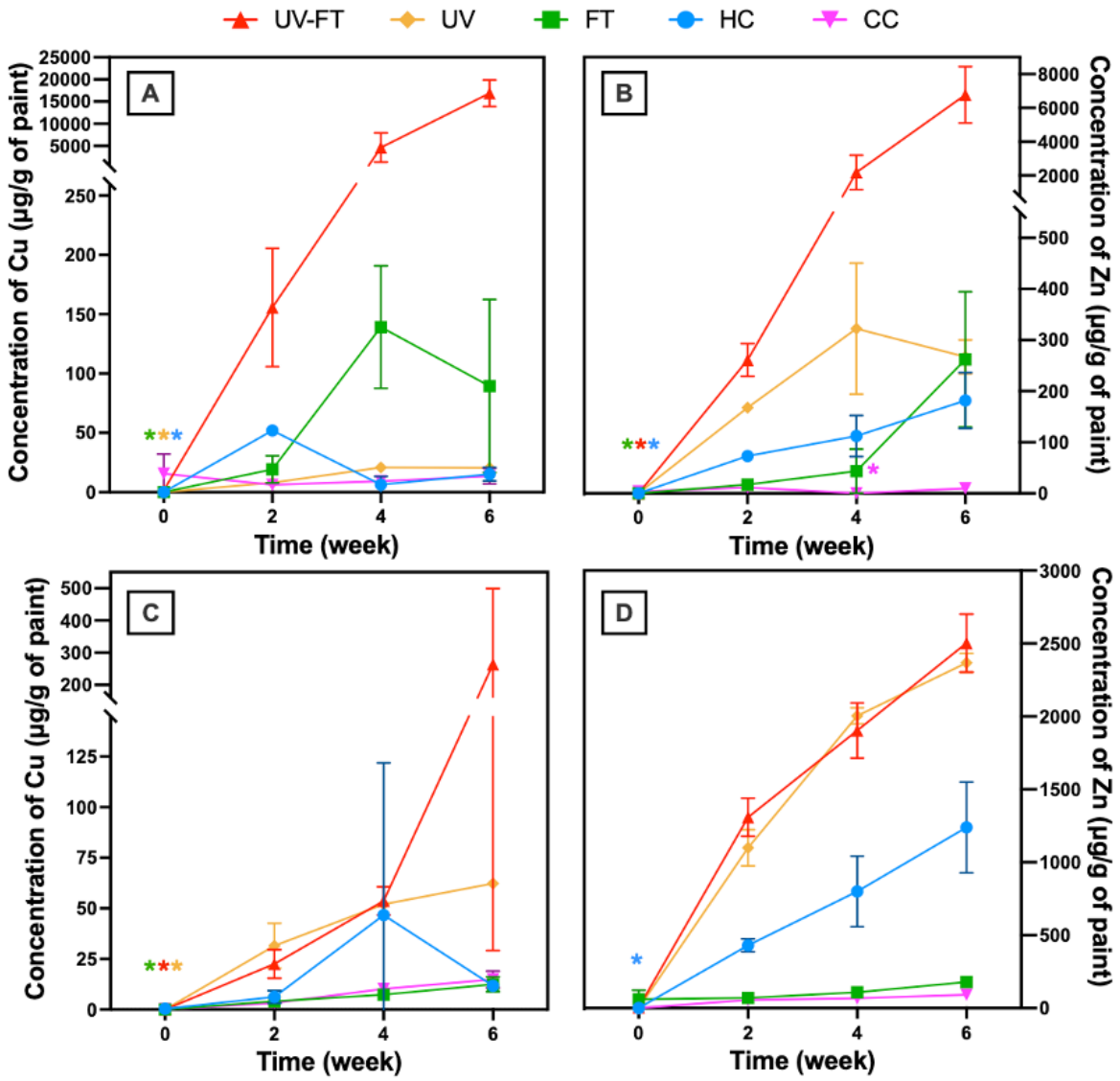

Figure 6. Average total Cu (left) and Zn (right) concentrations released from AF paint, in µg/g of dry paint, from three weathering treatments and two controls in F2 (>5 µm; A and B) and F3 (<5 µm; C and D). Concentrations were normalized to paint weights. Error bars denote the standard deviation around the mean of triplicate samples. Asterisks with their appropriate treatments denote values that are below the limit of detection and are attributed LOD/2.

The high metal concentrations in F2 for the UV-FT treatments were consistent with the high concentrations of paint particles that were found for this degradation condition. For F3, Cu was found at the highest concentration in the UV-FT fraction (260 ± 200 μg/g of dry paint), followed by UV (62 ± 3 μg/g of dry paint) whereas the release of Zn was similar for the two treatments (Figures 6C and D). Zn appeared to be more readily leached than Cu (Tables 3 and 4), similar to previous work in this field. For example, Simon et al. (2021) found that after 168 h, 0.2% of the total Cu had been leached from an AF paint as compared to 2.0% of the total Zn (Simon et al., 2021). Another study also found that ZnO was more readily leached than Cu_2O from AF paints that had different polymer binders (Jalaie et al., 2023). Because ZnO has a lower density compared to Cu_2O, it is liberated much quicker, allowing for more water penetration in the binder, which can in turn dissolve even more ZnO (Jalaie et al., 2023). In Figure 6D, the HC treatment released the next highest Zn concentrations in F3 after UV-FT and UV, however, we observed a decrease in pH the HC treatment during the six-week exposure (Figure A9A). Because ZnO has a propensity to dissolve in acidic environments (Yebra et al., 2006), this may be the cause for the high leaching in HC. The pH decrease might be attributed to the hydrolysis of Cu and other metals, such as aluminum (Simon et al., 2021), given that an increase in temperature can also increase Cu_2O dissolution.

2.3.4 Forms of Copper and Zinc Released From Paint

Cu and Zn concentrations in F3 were initially attributed to the leaching of dissolved metals from the paints. The concentrations of Cu and Zn released from the different weathering treatments and controls are given in Tables 3 and 4 for each of the 3 fractions for the six-week timepoint. UV-FT released the highest total masses of Cu and Zn (i.e., F1 + F2 + F3). As established before, the UV-FT treatment degraded the surface to the greatest extent.

Table 4. Masses of Cu released from five different treatments and controls at the 6-week timepoint. Concentrations ± standard deviation (µg of Cu) and the sum of each fraction (µg of Cu) are shown. The percentage of each fraction with respect to the total mass is also presented.

Weathering treatment	F1 (µg)	F2 (µg)	F3 (µg)	F1 + F2 + F3 (µg)	F1/(F1 + F2 + F3) (%)	F2/(F1 + F2 + F3) (%)	F3/(F1 + F2 + F3) (%)
CC	49 ± 30	0.22 ± 0.07	65 ± 20	110 ± 20	41.29	0.23	58.47
HC	160 ± 40	0.28 ± 0.10	50 ± 10	210 ± 20	75.79	0.13	24.07
UV	480 ± 200	0.39 ± 0.05	270 ± 12	750 ± 100	60.46	0.06	39.48
FT	19,000 ± 10,000	1.6 ± 1.0	56 ± 1	19,000 ± 7,000	99.64	0.01	0.34
UV-FT	220,000 ± 100,000	320 ± 60	1,200 ± 1,200	220,000 ± 70,000	99.36	0.16	0.47

Table 5. Masses of Zn released from five different treatments and controls at the 6-week timepoint. Concentrations ± standard deviation (µg of Zn) and the sum of each fraction ± standard deviation (µg of Zn) are shown. The percentage of each fraction with respect to the total mass is also presented.

Weathering treatment	F1 (µg)	F2 (µg)	F3 (µg)	F1 + F2 + F3 (µg)	F1/(F1 + F2 + F3) (%)	F2/(F1 + F2 + F3) (%)	F3/(F1 + F2 + F3) (%)
CC	51 ± 70	0.17 ± 0.06	400 ± 200	450 ± 100	9.97	0.04	89.99
HC	46 ± 5	3 ± 1	5,300 ± 1,000	5400 ± 700	0.89	0.06	99.05
UV	130 ± 70	5 ± 0.7	10,000 ± 300	10,000 ± 200	1.29	0.05	98.66
FT	5,700 ± 4,000	4 ± 2	810 ± 200	6,500 ± 2,000	85.56	0.08	14.36
UV-FT	66,000 ± 40,000	130 ± 30	11,000 ± 400	78,000 ± 20,000	83.46	0.18	16.36

For most treatments, Cu was mostly released in F1 (large particles), while a majority of Zn was released in F3 (<5 µm) (Tables 4 and 5), demonstrating that Cu was more likely to stay in the paint microparticles, whereas Zn had a higher propensity to be immediately released through leaching, especially for non-abrasive treatments (UV, HC, and CC). Since ZnO has a lower molar mass and lower density than Cu_2O, it may have been liberated much faster from the paint binder (Jalaie et al., 2023). Although this suggests that Zn was released in dissolved form, Miller et al. (2020) showed that Zn could be released from paints in its particulate form (bulk and nanoparticle)

in the initial hours of a water submersion. After those first few hours, the particulate Zn then quickly dissolved. Although our data is lacking hour-by-hour concentrations, the decreased pHs measured after two weeks for UV, HC, CC and UV-FT support the hypothesis that Zn was mostly present in its dissolved forms in F3 (Figure A9A).

2.3.5 Release of Nanoparticles From Paint

Copper oxide (I), or Cu_2O, nanoparticles have also been shown to be released from AF paints (Adeleye et al., 2016). Though Cu_2O comprised 30-60% of the total weight of the paint used here (Table A1), the manufacturer did not specifically state if it was added in a nanoparticle form. Measurements by SP-ICP-MS showed clearly that Cu-containing nanoparticles could be detected in F3, for the FT and CC treatments (Figure A13).

By assuming a spherical shape and density of 6.0 g/cm^3 corresponding to Cu_2O, it was possible to estimate that ($(1.6 \pm 1.1) \times 10^8$ Cu_2O nanoparticles/g of dry paint for the FT-exposed surfaces. After four weeks, the number concentration decreased ($(4.4 \pm 3.6) \times 10^7$ Cu_2O nanoparticles/g of dry paint) and it was ultimately below the limit of detection at six weeks (Figure A13). Cu_2O nanoparticles were also detected in CC-exposed coupons, but only at the two-week timepoint ($(9.91 \pm 5.64) \times 10^5$ Cu_2O particles/g of dry paint).

The size distributions of Cu_2O nanoparticles generated by the AF treatment were determined. The size distribution of the nanoparticles was found to be similar for both timepoints in the FT treatment, with a mean diameter of 30 ± 1 nm and 29 ± 1 nm for two and four weeks, respectively (Figure 7). For CC treatment at two weeks, Cu_2O nanoparticles had larger particle sizes (average median 61 ± 2 nm). The size range of Cu_2O nanoparticles released from paint is similar to what has been observed in earlier studies. For example, Gondikas et al. (2023) reported that the majority of Cu nanoparticles in marinas were approximately 45 nm in size. Similarly,

Adeleye et al. (2016) observed that 44 nm was the most commonly detected particle size for Cu_2O nanoparticles released from antifouling paints exposed to laboratory-controlled weathering. The larger size distribution in CC suggests that the Cu_2O nanoparticles had aged, leading to loss of nanoparticles via coalescence or aggregation.

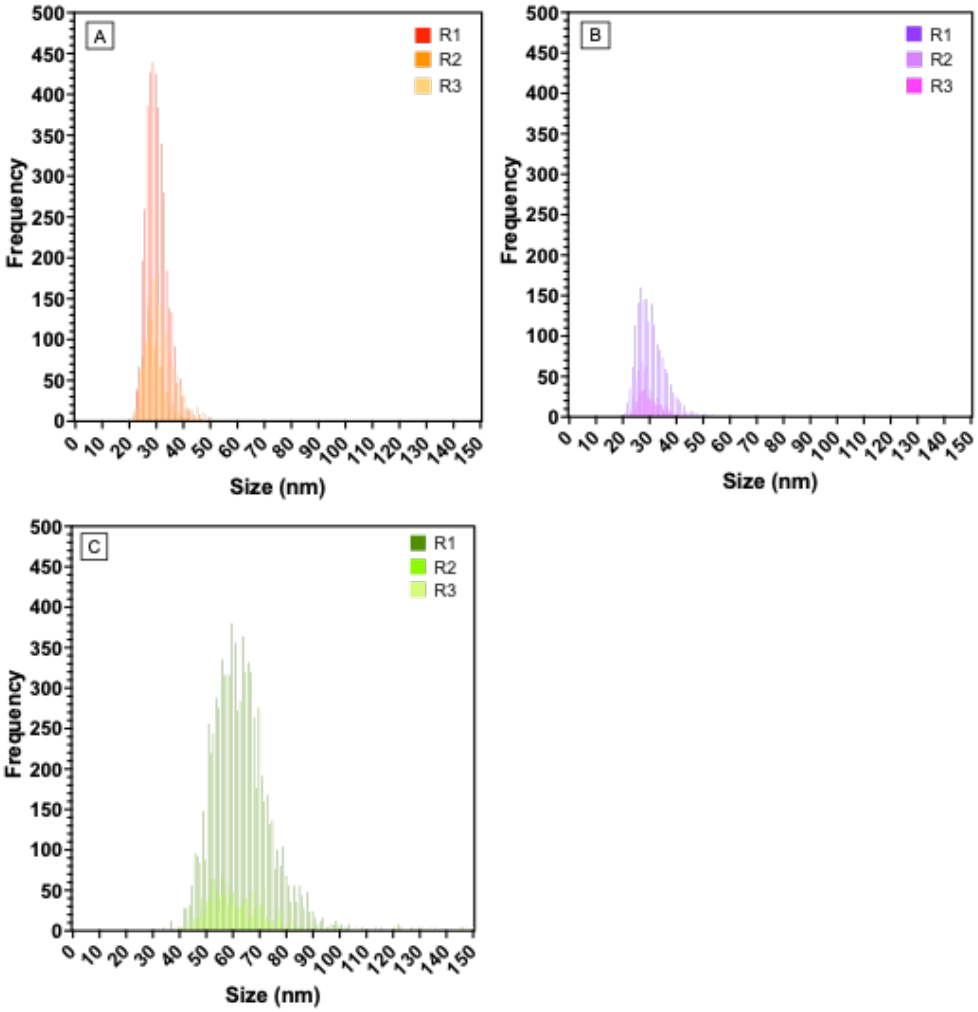

Figure 7. Size distribution (nm) of Cu_2O nanoparticles released from AF paints exposed to (A) the FT treatment after two weeks; (B) the FT treatment after four weeks; and (C) CC after two weeks. Bin width is equal to 1 and bin values from 151 to 707 were omitted for clarity. The legend indicates the triplicate samples (n = 3) measured for each time point.

The low detection rates of Cu_2O (and ZnO) nanoparticles could be the result of the peak signals (nanoparticles), being overwhelmed by the signal intensity of the dissolved background

(raw data provided in Figure A14). Indeed, mass concentrations of the dissolved metals were generally much higher than concentrations of the nanoparticles (Table A7). As such, most of the nanoparticle peaks could have been "hidden" by the background, as demonstrated in the raw signal data. This result is consistent with our total metals analysis for F3. An extremely high concentration of Cu was measured in F3 for the UV-FT treatment, indicating that it was likely that most of the Cu was released in its dissolved form (Figure 6C). Additionally, UV and HC treatments had relatively high concentrations of Cu in F3. High dissolved backgrounds for UV-FT, UV and HC may be caused by heat, increasing the dissolution of Cu in water. In comparison, FT and CC had the lowest concentrations of Cu in F3 (Figure 6C) and these were also the only treatments nanoparticles were detected (Figure A13).

2.4 Conclusions

Paint particles were generated in all weathering treatments and controls and were found to be released at the highest quantities in the UV-FT treatment. Chemical changes in the paint binder were detected in the UV exposed coupons, but not the generated paint particles. Paint particles generated from the UV-only treatment had a low similarity to the corresponding weathered coupon where UV irradiation may have weakened the paint binder via hydroxylation of unsaturated functional groups. For freeze-thaw, ice abrasion likely degraded the painted surface. Nonetheless, both mechanisms resulted in the release of paint particles. For combined UV radiation and freeze-thaw cycles, a synergistic effect appeared to take place, generating large and abundant paint particles.

Cu and Zn, major biocides used in antifouling paints, were released at the highest levels in UV-FT conditions. High levels of Cu and Zn from antifouling paint have been shown to be toxic to non-target organisms (Muller-Karanassos et al., 2021; Soroldoni et al., 2020; Turner et al., 2009;

Ytreberg et al., 2010). Thus, our findings impart negative implications for Cu and Zn pollution in the aquatic environment. Additionally, our results give evidence for the release of Cu_2O nanoparticles from antifouling paints. Studies have shown that Cu_2O nanoparticles can be toxic to aquatic organisms since they can transform into their ionic form, thus increasing their bioavailability (Chen et al., 2011; Miller et al., 2020; Wang et al., 2015). As such, antifouling paints can be a significant source of anthropogenic nanoparticle pollution.

The findings from this study advance our understanding of the fate of plastics and metals released from antifouling and self-polishing paints in the environment and their underlying mechanisms. Given the inevitability of paint pollution, it is crucial to promote the use of sustainable alternatives, reduce paint use and improve paint management practices to mitigate the pervasive problem stemming from marine paint contamination.

Chapter 3: Conclusions and Future Work

3.1 Conclusions

The field of paint pollution has grown in recent years, but data on the behaviour and fate of paints in relevant environmental contexts are still lacking. This thesis aimed to address these knowledge gaps by exposing antifouling painted surfaces to different simulated environmental conditions, and then characterizing and quantifying the contaminants (i.e., microplastics, nanoparticles, and metals) released from the painted surfaces. From our experimental results, the mechanisms behind the release of microplastics and metals were determined. The main objectives and their conclusions were as follows:

1) **Our first objective sought to determine the effect of weathering over time on painted surfaces.** All treatments (UV, FT and UV-FT) and controls (CC and HC) studied released microplastics and metals due to the nature of the paint used, which was antifouling and self-polishing. We highlighted that the treatment with the combination of UV and freeze-thaw (UV-FT) exposure released the highest quantities of microplastics and total metals from AF paint.
2) **Our second objective was to characterize and quantify microplastics and metals released from the painted surfaces.** We confirmed the identity of the paint particles, i.e., microplastics using O-PTIR, by comparing it to the reference antifouling paint used. The largest particles were generated in the UV-FT treatment, owing mostly to the effect of freeze-thaw. The highest amount of paint particles was also found in the same treatment, most likely due to the degrading effect of UV radiation.

   Cu and Zn are extensively used in antifouling paint due to their biocidal properties and relevant levels have been detected in many environmental studies. As such, our study

focused on their detection using ICP-MS. We found that Cu and Zn concentrations were the highest in the UV-FT treatment. Conditions involving freeze-thaw released the highest concentrations of Cu (i.e., UV-FT and FT) due to the high number of paint particles generated. We also investigated the possible release of nanoparticles. We detected Cu_2O nanoparticles with SP-ICP-MS but only in two conditions (FT and CC). Our results showed evidence that the nanoparticle peaks were hidden by the dissolved background.

3) **The third objective was to identify possible mechanisms for degradation of the painted surface.** Ice abrasion was the main mechanism for which freeze-thaw conditions generated high amounts and the largest paint particles, i.e., microplastics. UV radiation, meanwhile, degraded the polymer binder by the formation of hydroxyl groups in unsaturated functional groups, leading to the breakdown of paint into microplastics. Ergo, a synergistic effect can occur for the combined UV and freeze-thaw treatment, weakening the paint binder, and generating paint microplastics.

   For metal release, Cu tended to remain in the paint particles, hence why a high concentration of Cu was released in conditions that produced many paint particles (e.g., UV-FT and FT). Meanwhile, Zn was more likely to be released in its dissolved form when exposed to conditions involving heat (i.e., UV and HC). Zn was not tightly bound to the paint matrix, allowing it to be released in its particulate form before quickly dissolving.

4) **The last objective was to establish methodologies and techniques to characterize and quantify microplastics and metals released from paints.** We used a combination of techniques to achieve this objective. For paint particles, i.e., microplastics, we used O-PTIR and microscopy to confirm their chemical identity and determine their quantity. For metals, ICP-MS detected the relevant metals for analysis and calculated their actual

concentrations. SP-ICP-MS gave evidence for the presence of metal nanoparticles, particularly Cu_2O nanoparticles. It must be noted that these techniques were appropriate for samples generated in the laboratory.

The results of this thesis confirm that painted surfaces can be a source of microplastic and metal pollution. The large body of literature showing the potential ecotoxicity of microplastics and metals derived from paint highlight that these contaminants should be a significant concern given they are intentionally released into the environment to target specific organisms. Inevitably, this can have negative consequences for non-target species.

3.2 Perspectives and Future Work

Our work presented a framework for other researchers to analyze metals and microplastics released from painted surfaces after exposure to different weathering conditions. We outlined a variety of techniques that can successfully quantify and characterize microplastics released from paints down to 5 μm. The combination of techniques can also determine the fate of metals (i.e., dissolved or particulate) by assuming that size fractions smaller than 5 μm were mostly composed of dissolved metals and nanoparticles whereas fractions larger than this were particulate metals retained in paint particles.

The current thesis does have its limitations. Future work should consider other weathering exposure conditions relevant to paint applications. Marine yacht paint was the paint used in this thesis, and therefore the influence of mechanical weathering conditions such as movement in water should be considered. Simulating the effect of water erosion can give better insight into the degradation of the paints applied to marine vessels. Additionally, some parameters in this study are a simplification of what is found in the environment. For example, the water used in the current study was demineralized water, which, as implied by the name, does not include any minerals or

impurities. Demineralized water was used to ensure contaminant microplastics were filtered out and possible interferences for the metals analyzed were removed. Future analyses should consider complex and environmentally relevant waters such as natural waters, as well as the effects of different pHs, salinities and total organic carbon present in real natural waters. It is expected that degradation mechanisms will differ widely across different natural waters. For example, salts in sea water can interact with metals, leading to faster hydrolysis and a different degradation mechanism. Future studies should also undertake the use of other types and brands of marine paint to assess other possible paint degradation mechanisms.

Other analytical techniques can be applied for paint weathering studies to give a more holistic picture of the mechanism of paint release. For example, nanoplastics was not considered in this analysis. Therefore, scanning electron microscopy with energy dispersive X-ray spectroscopy (SEM-EDX) can be a helpful technique to determine size and shape of nano-sized paint particles, whilst also looking at the metal content. In the same vein, other engineered metal nanoparticles can also be analyzed in future studies. ZnO was not chosen for SP-ICP-MS analysis due to the high Zn dissolved content; therefore, a resin can be used to lower the dissolved ionic background and detect ZnO nanoparticles.

For determining degradation mechanisms in the polymeric paint binder, X-ray diffraction analysis can be used as it gives information on the chemical and physical properties of paint. This technique can also give quantitative information on inorganic pigments and extenders in unknown samples (Debnath & Vaidya, 2006). Another X-ray technique that has been used in the characterization of paints is X-ray photoelectron spectroscopy, which analyzes paint surface chemistry (Aziz & Ismail, 2017). It not only gives the elemental information but also the chemical state of these elements. Therefore, this technique can give information on the type of metal species

present and their eventual fate (Adeleye et al., 2016). Lastly, atomic force microscopy (AFM) has been used to determine the surface roughness of paints (Kang et al., 2025). AFM can give insight into the degradation of painted surfaces after weathering at the nanoscale.

To give a more holistic picture of the fate and transport of the paint particles, field work can also be done. For example, samples at sites where boat maintenance are taking place could be taken and analysed. This has been done in a few studies that looked at the extent of metal pollution from paints within an area (Eklund et al., 2014; Soroldoni et al., 2018; Turner et al., 2015). This gives a clearer picture as to where the paint particles are coming from and if any changes are happening due to environmental exposure.

The results of this work emphasize that paint particles can be a source of microplastics and metal pollution to the environment. The weathering treatments used in this study are more simplified, ergo, environmental conditions in a natural environment may have more drastic effects on the degradation of paint and its release products. This, and other studies, motivate the need for more sustainable alternatives to existing antifouling paints. However, paint pollution will continue to persist, even if a complete switch to more sustainable alternatives is made. Mitigation strategies and reduction of paint use should be an area of focus for both users and manufacturers.

References

Abbasi, S., Soltani, N., Keshavarzi, B., Moore, F., Turner, A., & Hassanaghaei, M. (2018). Microplastics in different tissues of fish and prawn from the Musa Estuary, Persian Gulf. *Chemosphere*, *205*, 80–87. https://doi.org/10.1016/j.chemosphere.2018.04.076

Abd Mutalib, M., Rahman, M. A., Othman, M. H. D., Ismail, A. F., & Jaafar, J. (2017). Scanning Electron Microscopy (SEM) and Energy-Dispersive X-Ray (EDX) Spectroscopy. In *Membrane Characterization* (pp. 161–179). Elsevier. https://doi.org/10.1016/B978-0-444-63776-5.00009-7

Abd Rashid, N., Salim, Y. S., Abdul Halim, S. I., Harun, M. K., Ong, C. H., & Chan, C. H. (2023). FTIR conformity analysis and performance testings of fresh, aged and expired polymeric paints under different storage conditions. *Pure and Applied Chemistry*, *95*(2), 81–98. https://doi.org/10.1515/pac-2022-0901

Adeleye, A. S., Oranu, E. A., Tao, M., & Keller, A. A. (2016). Release and detection of nanosized copper from a commercial antifouling paint. *Water Research*, *102*, 374–382. https://doi.org/10.1016/j.watres.2016.06.056

Akzonobel. (2017). *Which type of antifouling should I use on my boat?* International Yacht Paint. https://www.international-yachtpaint.com/en/ie/support/boat-paint-expert-advice/types-of-antifouling

Al-Kattan, A., Wichser, A., Vonbank, R., Brunner, S., Ulrich, A., Zuin, S., Arroyo, Y., Golanski, L., & Nowack, B. (2015). Characterization of materials released into water from paint containing nano-SiO2. *Chemosphere*, *119*, 1314–1321. https://doi.org/10.1016/j.chemosphere.2014.02.005

Al-Kattan, A., Wichser, A., Vonbank, R., Brunner, S., Ulrich, A., Zuin, S., & Nowack, B. (2013). Release of TiO2 from paints containing pigment-TiO2 or nano-TiO2 by weathering. *Environmental Science: Processes & Impacts*, *15*(12), 2186. https://doi.org/10.1039/c3em00331k

Araujo, C. F., Nolasco, M. M., Ribeiro, A. M. P., & Ribeiro-Claro, P. J. A. (2018). Identification of microplastics using Raman spectroscopy: Latest developments and future prospects. *Water Research*, *142*, 426–440. https://doi.org/10.1016/j.watres.2018.05.060

ASTM International. (1998). *Test Method for Testing Antifouling Panels in Shallow Submergence*. ASTM International. https://doi.org/10.1520/D3623-78AR98

ASTM International. (2020). *Test Method for Determination of Copper Release Rate From Antifouling Coatings in Substitute Ocean Water*. ASTM International. https://doi.org/10.1520/D6442-06R20

Azémard, C., Vieillescazes, C., & Ménager, M. (2014). Effect of photodegradation on the identification of natural varnishes by FT-IR spectroscopy. *Microchemical Journal*, *112*, 137–149. https://doi.org/10.1016/j.microc.2013.09.020

Azimzada, A., Farner, J. M., Hadioui, M., Liu-Kang, C., Jreije, I., Tufenkji, N., & Wilkinson, K. J. (2020a). Release of TiO 2 nanoparticles from painted surfaces in cold climates: characterization using a high sensitivity single-particle ICP-MS. *Environmental Science: Nano*, *7*(1), 139–148. https://doi.org/10.1039/C9EN00951E

Azimzada, A., Farner, J. M., Jreije, I., Hadioui, M., Liu-Kang, C., Tufenkji, N., Shaw, P., & Wilkinson, K. J. (2020b). Single- and Multi-Element Quantification and Characterization of TiO2 Nanoparticles Released From Outdoor Stains and Paints. *Frontiers in Environmental Science*, *8*. https://doi.org/10.3389/fenvs.2020.00091

Aziz, M., & Ismail, A. F. (2017). X-Ray Photoelectron Spectroscopy (XPS). In *Membrane Characterization* (pp. 81–93). Elsevier. https://doi.org/10.1016/B978-0-444-63776-5.00005-X

Biggs, T. W., & D'Anna, H. (2012). Rapid increase in copper concentrations in a new marina, San Diego Bay. *Marine Pollution Bulletin*, *64*(3), 627–635. https://doi.org/10.1016/j.marpolbul.2011.12.006

Bighiu, M. A., Eriksson-Wiklund, A. K., & Eklund, B. (2017a). Biofouling of leisure boats as a source of metal pollution. *Environmental Science and Pollution Research*, *24*(1), 997–1006. https://doi.org/10.1007/s11356-016-7883-7

Bighiu, M. A., Gorokhova, E., Carney Almroth, B., & Eriksson Wiklund, A.-K. (2017b). Metal contamination in harbours impacts life-history traits and metallothionein levels in snails. *PLOS ONE*, *12*(7), e0180157. https://doi.org/10.1371/journal.pone.0180157

Borges Ramirez, M. M., Dzul Caamal, R., & Rendón von Osten, J. (2019). Occurrence and seasonal distribution of microplastics and phthalates in sediments from the urban channel of the Ria and coast of Campeche, Mexico. *Science of The Total Environment*, *672*, 97–105. https://doi.org/10.1016/j.scitotenv.2019.03.472

Cardozo, A. L. P., Farias, E. G. G., Rodrigues-Filho, J. L., Moteiro, I. B., Scandolo, T. M., & Dantas, D. V. (2018). Feeding ecology and ingestion of plastic fragments by Priacanthus arenatus: What's the fisheries contribution to the problem? *Marine Pollution Bulletin*, *130*, 19–27. https://doi.org/10.1016/j.marpolbul.2018.03.010

Caron, A. G. M., Thomas, C. R., Berry, K. L. E., Motti, C. A., Ariel, E., & Brodie, J. E. (2018). Ingestion of microplastic debris by green sea turtles (Chelonia mydas) in the Great Barrier Reef: Validation of a sequential extraction protocol. *Marine Pollution Bulletin*, *127*, 743–751. https://doi.org/10.1016/j.marpolbul.2017.12.062

Chae, D.-H., Kim, I.-S., Kim, S.-K., Song, Y. K., & Shim, W. J. (2015). Abundance and Distribution Characteristics of Microplastics in Surface Seawaters of the Incheon/Kyeonggi Coastal Region. *Archives of Environmental Contamination and Toxicology*, *69*(3), 269–278. https://doi.org/10.1007/s00244-015-0173-4

Chen, D., Zhang, D., Yu, J. C., & Chan, K. M. (2011). Effects of Cu2O nanoparticle and CuCl2 on zebrafish larvae and a liver cell-line. *Aquatic Toxicology*, *105*(3–4), 344–354. https://doi.org/10.1016/j.aquatox.2011.07.005

Cunha, B., Garnier, J., Araújo, D., Tonhá, M., Souto-Oliveira, C. E., Ruiz, I., Feitas e Silva, F. H., Almeida, T., Freydier, R., Seyler, P., & Babinski, M. (2024). Metal record of copper-based antifouling paints in sediment core following marina construction and operation. *Marine Pollution Bulletin*, *204*, 116534. https://doi.org/10.1016/j.marpolbul.2024.116534

Debnath, N. C., & Vaidya, S. A. (2006). Application of X-ray diffraction technique for characterisation of pigments and control of paints quality. *Progress in Organic Coatings*, *56*(2–3), 159–168. https://doi.org/10.1016/j.porgcoat.2006.03.007

Dibke, C., Fischer, M., & Scholz-Böttcher, B. M. (2021). Microplastic Mass Concentrations and Distribution in German Bight Waters by Pyrolysis–Gas Chromatography–Mass Spectrometry/Thermochemolysis Reveal Potential Impact of Marine Coatings: Do Ships Leave Skid Marks? *Environmental Science & Technology*, *55*(4), 2285–2295. https://doi.org/10.1021/acs.est.0c04522

Eklund, B., Johansson, L., & Ytreberg, E. (2014). Contamination of a boatyard for maintenance of pleasure boats. *Journal of Soils and Sediments*, *14*(5), 955–967. https://doi.org/10.1007/s11368-013-0828-6

Faber, M., Marinković, M., de Valk, E., & Waaijers-van der Loop, S. L. (2021). *Paints and microplastics*. https://doi.org/10.21945/RIVM-2021-0060

Fang, C., Zhou, W., Hu, J., Wu, C., Niu, J., & Naidu, R. (2024). Paint has the potential to release microplastics, nanoplastics, inorganic nanoparticles, and hybrid materials. *Environmental Sciences Europe*, *36*(1), 17. https://doi.org/10.1186/s12302-024-00844-6

Germinario, G., van der Werf, I. D., & Sabbatini, L. (2016). Chemical characterisation of spray paints by a multi-analytical (Py/GC–MS, FTIR, μ-Raman) approach. *Microchemical Journal*, *124*, 929–939. https://doi.org/10.1016/j.microc.2015.04.016

Goenaga-Infante, H., & Bartczak, D. (2020). Single particle inductively coupled plasma mass spectrometry (spICP-MS). In *Characterization of Nanoparticles* (pp. 65–77). Elsevier. https://doi.org/10.1016/B978-0-12-814182-3.00003-1

Gondikas, A., Mattsson, K., & Hassellöv, M. (2023). Methods for the detection and characterization of boat paint microplastics in the marine environment. *Frontiers in Environmental Chemistry*, *4*. https://doi.org/10.3389/fenvc.2023.1090704

González-Cabrera, M., Domínguez-Vidal, A., & Ayora-Cañada, M. J. (2021). Monitoring UV-accelerated alteration processes of paintings by means of hyperspectral micro-FTIR imaging and chemometrics. *Spectrochimica Acta Part A: Molecular and Biomolecular Spectroscopy*, *253*, 119568. https://doi.org/10.1016/j.saa.2021.119568

Gosselin, C. A. (2024). *Marine Coatings: Striking a Balance in Biofouling Control*. American Coating Association. https://www.paint.org/coatingstech-magazine/articles/marine-coatings-striking-a-balance-in-biofouling-control/

Guimarães, R. H. E., Wallner-Kersanach, M., & Correa, J. A. M. (2022). Assessment of anthropogenic metals in shipyard sediment in the Amazon delta estuary in northern Brazil. *Environmental Science and Pollution Research*, *29*(51), 77007–77025. https://doi.org/10.1007/s11356-022-20960-1

Hayes, P. A., Vahur, S., & Leito, I. (2014). ATR-FTIR spectroscopy and quantitative multivariate analysis of paints and coating materials. *Spectrochimica Acta Part A: Molecular and Biomolecular Spectroscopy*, *133*, 207–213. https://doi.org/10.1016/j.saa.2014.05.058

Higgins, C., & Turner, A. (2023). Microplastics in surface coastal waters around Plymouth, UK, and the contribution of boating and shipping activities. *Science of The Total Environment*, *893*, 164695. https://doi.org/10.1016/j.scitotenv.2023.164695

Hobbs, W. O., McCall, M., Lanksbury, J., Seiders, K., Sandvik, P., Jones, M., Chuhran, H., Momohara, D., & Norton, D. (2022). A baseline of copper associated with antifouling paint in marinas within a large fjord estuary. *Marine Pollution Bulletin*, *178*, 113547. https://doi.org/10.1016/j.marpolbul.2022.113547

Holmes, L., & Turner, A. (2009). Leaching of hydrophobic Cu and Zn from discarded marine antifouling paint residues: Evidence for transchelation of metal pyrithiones. *Environmental Pollution*, *157*(12), 3440–3444. https://doi.org/10.1016/j.envpol.2009.06.018

Horton, A. A., Svendsen, C., Williams, R. J., Spurgeon, D. J., & Lahive, E. (2017). Large microplastic particles in sediments of tributaries of the River Thames, UK – Abundance, sources and methods for effective quantification. *Marine Pollution Bulletin*, *114*(1), 218–226. https://doi.org/10.1016/j.marpolbul.2016.09.004

Iliff, S. M., Wilczek, E. R., Harris, R. J., Bouldin, R., & Stoner, E. W. (2020). Evidence of microplastics from benthic jellyfish (Cassiopea xamachana) in Florida estuaries. *Marine Pollution Bulletin*, *159*, 111521. https://doi.org/10.1016/j.marpolbul.2020.111521

Imhof, H. K., Laforsch, C., Wiesheu, A. C., Schmid, J., Anger, P. M., Niessner, R., & Ivleva, N. P. (2016). Pigments and plastic in limnetic ecosystems: A qualitative and quantitative study on microparticles of different size classes. *Water Research*, *98*, 64–74. https://doi.org/10.1016/j.watres.2016.03.015

Ivar do Sul, J. A., Costa, M. F., & Fillmann, G. (2014). Microplastics in the pelagic environment around oceanic islands of the Western Tropical Atlantic Ocean. *Water, Air, & Soil Pollution*, *225*(7), 2004. https://doi.org/10.1007/s11270-014-2004-z

Jacobsen, S., Scherer, G. W., & Schulson, E. M. (2015). Concrete–ice abrasion mechanics. *Cement and Concrete Research*, *73*, 79–95. https://doi.org/10.1016/j.cemconres.2015.01.001

Jalaie, A., Afshaar, A., Mousavi, S. B., & Heidari, M. (2023). Investigation of the Release Rate of Biocide and Corrosion Resistance of Vinyl-, Acrylic-, and Epoxy-Based Antifouling Paints on Steel in Marine Infrastructures. *Polymers*, *15*(19), 3948. https://doi.org/10.3390/polym15193948

Jaouani, R., Mouneyrac, C., Châtel, A., Amiard, F., Dellali, M., Beyrem, H., Michelet, A., & Lagarde, F. (2022). Seasonal and spatial distribution of microplastics in sediments by FTIR imaging throughout a continuum lake - lagoon- beach from the Tunisian coast. *Science of The Total Environment*, *838*, 156519. https://doi.org/10.1016/j.scitotenv.2022.156519

Jessop, A., & Turner, A. (2011). Leaching of Cu and Zn from discarded boat paint particles into tap water and rain water. *Chemosphere*, *83*(11), 1575–1580. https://doi.org/10.1016/j.chemosphere.2011.01.021

Jin, H., Wang, J., Tian, L., Gao, M., Zhao, J., & Ren, L. (2022). Recent advances in emerging integrated antifouling and anticorrosion coatings. *Materials & Design*, *213*, 110307. https://doi.org/10.1016/j.matdes.2021.110307

Jost, C., Muehlethaler, C., & Massonnet, G. (2016). Forensic aspects of the weathering and ageing of spray paints. *Forensic Science International*, *258*, 32–40. https://doi.org/10.1016/j.forsciint.2015.11.001

Jreije, I., Azimzada, A., Hadioui, M., & Wilkinson, K. J. (2022). Stability of CeO 2 nanoparticles from paints and stains: insights under controlled and environmental scenarios. *Environmental Science: Nano*, *9*(9), 3361–3371. https://doi.org/10.1039/D2EN00210H

Kaegi, R., Sinnet, B., Zuleeg, S., Hagendorfer, H., Mueller, E., Vonbank, R., Boller, M., & Burkhardt, M. (2010). Release of silver nanoparticles from outdoor facades. *Environmental Pollution*, *158*(9), 2900–2905. https://doi.org/10.1016/j.envpol.2010.06.009

Kaegi, R., Ulrich, A., Sinnet, B., Vonbank, R., Wichser, A., Zuleeg, S., Simmler, H., Brunner, S., Vonmont, H., Burkhardt, M., & Boller, M. (2008). Synthetic TiO2 nanoparticle emission from

exterior facades into the aquatic environment. *Environmental Pollution*, *156*(2), 233–239. https://doi.org/10.1016/j.envpol.2008.08.004

Kalogerakis, N., Karkanorachaki, K., Kalogerakis, G. C., Triantafyllidi, E. I., Gotsis, A. D., Partsinevelos, P., & Fava, F. (2017). Microplastics Generation: Onset of Fragmentation of Polyethylene Films in Marine Environment Mesocosms. *Frontiers in Marine Science*, *4*. https://doi.org/10.3389/fmars.2017.00084

Kang, J.-H., Kwon, O. Y., Lee, K.-W., Song, Y. K., & Shim, W. J. (2015). Marine neustonic microplastics around the southeastern coast of Korea. *Marine Pollution Bulletin*, *96*(1–2), 304–312. https://doi.org/10.1016/j.marpolbul.2015.04.054

Kang, Y., Jo, H. H., & Kim, S. (2025). Effects of UV degradation on building materials with emphasis on microplastic generation potential. *Journal of Hazardous Materials*, *483*, 136521. https://doi.org/10.1016/j.jhazmat.2024.136521

Käppler, A., Windrich, F., Löder, M. G. J., Malanin, M., Fischer, D., Labrenz, M., Eichhorn, K.-J., & Voit, B. (2015). Identification of microplastics by FTIR and Raman microscopy: a novel silicon filter substrate opens the important spectral range below 1300 cm−1 for FTIR transmission measurements. *Analytical and Bioanalytical Chemistry*, *407*(22), 6791–6801. https://doi.org/10.1007/s00216-015-8850-8

Katranitsas, A., Castritsi-Catharios, J., & Persoone, G. (2003). The effects of a copper-based antifouling paint on mortality and enzymatic activity of a non-target marine organism. *Marine Pollution Bulletin*, *46*(11), 1491–1494. https://doi.org/10.1016/S0025-326X(03)00253-4

Kwon, O. Y., Kang, J.-H., Hong, S. H., & Shim, W. J. (2020). Spatial distribution of microplastic in the surface waters along the coast of Korea. *Marine Pollution Bulletin*, *155*, 110729. https://doi.org/10.1016/j.marpolbul.2019.110729

Lacerda, A. L. d. F., Rodrigues, L. dos S., van Sebille, E., Rodrigues, F. L., Ribeiro, L., Secchi, E. R., Kessler, F., & Proietti, M. C. (2019). Plastics in sea surface waters around the Antarctic Peninsula. *Scientific Reports*, *9*(1), 3977. https://doi.org/10.1038/s41598-019-40311-4

Lagerström, M., Strand, J., Eklund, B., & Ytreberg, E. (2017). Total tin and organotin speciation in historic layers of antifouling paint on leisure boat hulls. *Environmental Pollution*, *220*, 1333–1341. https://doi.org/10.1016/j.envpol.2016.11.001

Lagerström, M., & Ytreberg, E. (2021). Quantification of Cu and Zn in antifouling paint films by XRF. *Talanta*, *223*, 121820. https://doi.org/10.1016/j.talanta.2020.121820

Laist, D. W. (1997). *Impacts of Marine Debris: Entanglement of Marine Life in Marine Debris Including a Comprehensive List of Species with Entanglement and Ingestion Records* (pp. 99–139). https://doi.org/10.1007/978-1-4613-8486-1_10

Leistenschneider, C., Burkhardt-Holm, P., Mani, T., Primpke, S., Taubner, H., & Gerdts, G. (2021). Microplastics in the Weddell Sea (Antarctica): A Forensic Approach for Discrimination between Environmental and Vessel-Induced Microplastics. *Environmental Science & Technology*, *55*(23), 15900–15911. https://doi.org/10.1021/acs.est.1c05207

Lima, A. R. A., Costa, M. F., & Barletta, M. (2014). Distribution patterns of microplastics within the plankton of a tropical estuary. *Environmental Research*, *132*, 146–155. https://doi.org/10.1016/j.envres.2014.03.031

Lockwood, T. (2024). *SPCal*. https://spcal.readthedocs.io/en/latest/

Macali, A., Semenov, A., Venuti, V., Crupi, V., D'Amico, F., Rossi, B., Corsi, I., & Bergami, E. (2018). Episodic records of jellyfish ingestion of plastic items reveal a novel pathway for trophic transference of marine litter. *Scientific Reports*, *8*(1), 6105. https://doi.org/10.1038/s41598-018-24427-7

Mani, T., Primpke, S., Lorenz, C., Gerdts, G., & Burkhardt-Holm, P. (2019). Microplastic Pollution in Benthic Midstream Sediments of the Rhine River. *Environmental Science & Technology*, *53*(10), 6053–6062. https://doi.org/10.1021/acs.est.9b01363

Marrion, A., & Guy, A. (2004). Coatings components beyond binders. In A. Marrion (Ed.), *The Chemistry and Physics of Coatings* (p. 50). The Royal Society of Chemistry. https://doi.org/10.1039/9781847558206

Mengatto, M. F., & Nagai, R. H. (2022). A first assessment of microplastic abundance in sandy beach sediments of the Paranaguá Estuarine Complex, South Brazil (RAMSAR site). *Marine Pollution Bulletin*, *177*, 113530. https://doi.org/10.1016/j.marpolbul.2022.113530

Miller, R. J., Adeleye, A. S., Page, H. M., Kui, L., Lenihan, H. S., & Keller, A. A. (2020). Nano and traditional copper and zinc antifouling coatings: metal release and impact on marine sessile invertebrate communities. *Journal of Nanoparticle Research*, *22*(5), 129. https://doi.org/10.1007/s11051-020-04875-x

Müller, A.-K., Brehm, J., Völkl, M., Jérôme, V., Laforsch, C., Freitag, R., & Greiner, A. (2022a). Disentangling biological effects of primary nanoplastics from dispersion paints' additional compounds. *Ecotoxicology and Environmental Safety*, *242*, 113877. https://doi.org/10.1016/j.ecoenv.2022.113877

Müller, A.-K., Brehm, J., Völkl, M., Jérôme, V., Laforsch, C., Freitag, R., & Greiner, A. (2022b). Disentangling biological effects of primary nanoplastics from dispersion paints' additional compounds. *Ecotoxicology and Environmental Safety*, *242*, 113877. https://doi.org/10.1016/j.ecoenv.2022.113877

Muller-Karanassos, C., Arundel, W., Lindeque, P. K., Vance, T., Turner, A., & Cole, M. (2021). Environmental concentrations of antifouling paint particles are toxic to sediment-dwelling

invertebrates. *Environmental Pollution*, *268*, 115754. https://doi.org/10.1016/j.envpol.2020.115754

Muller-Karanassos, C., Turner, A., Arundel, W., Vance, T., Lindeque, P. K., & Cole, M. (2019). Antifouling paint particles in intertidal estuarine sediments from southwest England and their ingestion by the harbour ragworm, Hediste diversicolor. *Environmental Pollution*, *249*, 163–170. https://doi.org/10.1016/j.envpol.2019.03.009

Neves, D., Sobral, P., Ferreira, J. L., & Pereira, T. (2015). Ingestion of microplastics by commercial fish off the Portuguese coast. *Marine Pollution Bulletin*, *101*(1), 119–126. https://doi.org/10.1016/j.marpolbul.2015.11.008

OECD. (2014). *Coating Industry (Paints, Lacquers and Varnishes)*. OECD. https://doi.org/10.1787/9789264221093-en

Omae, I. (2003). Organotin antifouling paints and their alternatives. *Applied Organometallic Chemistry*, *17*(2), 81–105. https://doi.org/10.1002/aoc.396

Ory, N. C., Sobral, P., Ferreira, J. L., & Thiel, M. (2017). Amberstripe scad Decapterus muroadsi (Carangidae) fish ingest blue microplastics resembling their copepod prey along the coast of Rapa Nui (Easter Island) in the South Pacific subtropical gyre. *Science of The Total Environment*, *586*, 430–437. https://doi.org/10.1016/j.scitotenv.2017.01.175

Paruta, P., Pucino, M., & Boucher, J. B. (2022). *Plastic Paints the Environment*.

Philipp, C., Unger, B., Ehlers, S. M., Koop, J. H. E., & Siebert, U. (2021). First Evidence of Retrospective Findings of Microplastics in Harbour Porpoises (Phocoena phocoena) From German Waters. *Frontiers in Marine Science*, *8*. https://doi.org/10.3389/fmars.2021.682532

Pilcher, G. R. (2023). *The State of the U.S. Paint and Coatings Market: More Reliable Supply Chain, Slight Decline in Volume*.

Primpke, S., Cross, R. K., Mintenig, S. M., Simon, M., Vianello, A., Gerdts, G., & Vollertsen, J. (2020). Toward the Systematic Identification of Microplastics in the Environment: Evaluation of a New Independent Software Tool (siMPle) for Spectroscopic Analysis. *Applied Spectroscopy*, *74*(9), 1127–1138. https://doi.org/10.1177/0003702820917760

Russell, D. J., Hargrove, S., & Balazs, G. H. (2011). Marine Sponges, Other Animal Food, and Nonfood Items Found in Digestive Tracts of the Herbivorous Marine Turtle Chelonia mydas in Hawai'i. *Pacific Science*, *65*(3), 375–381. https://doi.org/10.2984/65.3.375

Schlotter, N. E. (1989). Raman Spectroscopy. In *Comprehensive Polymer Science and Supplements* (pp. 469–497). Elsevier. https://doi.org/10.1016/B978-0-08-096701-1.00021-5

Sileo, L., & Fefer, S. I. (1987). PAINT CHIP POISONING OF LAYSAN ALBATROSS AT MIDWAY ATOLL. *Journal of Wildlife Diseases*, *23*(3), 432–437. https://doi.org/10.7589/0090-3558-23.3.432

Simon, M., Vianello, A., Shashoua, Y., & Vollertsen, J. (2021). Accelerated weathering affects the chemical and physical properties of marine antifouling paint microplastics and their identification by ATR-FTIR spectroscopy. *Chemosphere*, *274*, 129749. https://doi.org/10.1016/j.chemosphere.2021.129749

Singh, N., & Turner, A. (2009a). Leaching of copper and zinc from spent antifouling paint particles. *Environmental Pollution*, *157*(2), 371–376. https://doi.org/10.1016/j.envpol.2008.10.003

Singh, N., & Turner, A. (2009b). Trace metals in antifouling paint particles and their heterogeneous contamination of coastal sediments. *Marine Pollution Bulletin*, *58*(4), 559–564. https://doi.org/10.1016/j.marpolbul.2008.11.014

Sobhani, Z., Zhang, X., Gibson, C., Naidu, R., Megharaj, M., & Fang, C. (2020). Identification and visualisation of microplastics/nanoplastics by Raman imaging (i): Down to 100 nm. *Water Research*, *174*, 115658. https://doi.org/10.1016/j.watres.2020.115658

Song, Y. K., Hong, S. H., Jang, M., Kang, J.-H., Kwon, O. Y., Han, G. M., & Shim, W. J. (2014). Large Accumulation of Micro-sized Synthetic Polymer Particles in the Sea Surface Microlayer. *Environmental Science & Technology*, *48*(16), 9014–9021. https://doi.org/10.1021/es501757s

Soon, Z. Y., Jung, J.-H., Loh, A., Yoon, C., Shin, D., & Kim, M. (2021). Seawater contamination associated with in-water cleaning of ship hulls and the potential risk to the marine environment. *Marine Pollution Bulletin*, *171*, 112694. https://doi.org/10.1016/j.marpolbul.2021.112694

Soroldoni, S., Castro, Í. B., Abreu, F., Duarte, F. A., Choueri, R. B., Möller, O. O., Fillmann, G., & Pinho, G. L. L. (2018). Antifouling paint particles: Sources, occurrence, composition and dynamics. *Water Research*, *137*, 47–56. https://doi.org/10.1016/j.watres.2018.02.064

Soroldoni, S., Honscha, L. C., Reis, F. O., Duarte, F. A., da Silva, F. M. R., & Pinho, G. L. L. (2021). Antifouling paint particles in soils: toxic impact that goes beyond the aquatic environment. *Ecotoxicology*, *30*(6), 1161–1169. https://doi.org/10.1007/s10646-021-02418-1

Soroldoni, S., Vieira da Silva, S., Castro, Í. B., de Martinez Gaspar Martins, C., & Leães Pinho, G. L. (2020). Antifouling paint particles cause toxicity to benthic organisms: Effects on two species with different feeding modes. *Chemosphere*, *238*, 124610. https://doi.org/10.1016/j.chemosphere.2019.124610

Subramanian, A., & Rodriguez-Saona, L. (2009). Fourier Transform Infrared (FTIR) Spectroscopy. In *Infrared Spectroscopy for Food Quality Analysis and Control* (pp. 145–178). Elsevier. https://doi.org/10.1016/B978-0-12-374136-3.00007-9

Tang, C. Y., & Yang, Z. (2017). Transmission Electron Microscopy (TEM). In *Membrane Characterization* (pp. 145–159). Elsevier. https://doi.org/10.1016/B978-0-444-63776-5.00008-5

Tang, C.-C., Chen, H.-I., Brimblecombe, P., & Lee, C.-L. (2018). Textural, surface and chemical properties of polyvinyl chloride particles degraded in a simulated environment. *Marine Pollution Bulletin*, *133*, 392–401. https://doi.org/10.1016/j.marpolbul.2018.05.062

Thomas, M. (2016). The durability of concrete for marine construction. In *Marine Concrete Structures* (pp. 151–170). Elsevier. https://doi.org/10.1016/B978-0-08-100081-6.00006-4

Torres, F. G., & De-la-Torre, G. E. (2021). Environmental pollution with antifouling paint particles: Distribution, ecotoxicology, and sustainable alternatives. *Marine Pollution Bulletin*, *169*, 112529. https://doi.org/10.1016/j.marpolbul.2021.112529

Turner, A. (2010). Marine pollution from antifouling paint particles. *Marine Pollution Bulletin*, *60*(2), 159–171. https://doi.org/10.1016/j.marpolbul.2009.12.004

Turner, A. (2021). Paint particles in the marine environment: An overlooked component of microplastics. *Water Research X*, *12*, 100110. https://doi.org/10.1016/j.wroa.2021.100110

Turner, A., Comber, S., Rees, A. B., Gkiokas, D., & Solman, K. (2015). Metals in boat paint fragments from slipways, repair facilities and abandoned vessels: An evaluation using field portable XRF. *Talanta*, *131*, 372–378. https://doi.org/10.1016/j.talanta.2014.08.012

Turner, A., Ostle, C., & Wootton, M. (2022). Occurrence and chemical characteristics of microplastic paint flakes in the North Atlantic Ocean. *Science of the Total Environment*, *806*, 150375. https://doi.org/10.1016/j.scitotenv.2021.150375

Turner, A., Pollock, H., & Brown, M. T. (2009). Accumulation of Cu and Zn from antifouling paint particles by the marine macroalga, Ulva lactuca. *Environmental Pollution*, *157*(8–9), 2314–2319. https://doi.org/10.1016/j.envpol.2009.03.026

van der Weerd, J., van Loon, A., & Boon, J. J. (2005). FTIR Studies of the Effects of Pigments on the Aging of Oil. *Studies in Conservation*, *50*(1), 3–22. https://doi.org/10.1179/sic.2005.50.1.3

Wang, H., Fan, W., Xue, F., Wang, X., Li, X., & Guo, L. (2015). Chronic effects of six micro/nano-Cu2O crystals with different structures and shapes on Daphnia magna. *Environmental Pollution*, *203*, 60–68. https://doi.org/10.1016/j.envpol.2015.03.043

Wilschefski, S., & Baxter, M. (2019). Inductively Coupled Plasma Mass Spectrometry: Introduction to Analytical Aspects. *Clinical Biochemist Reviews*, *40*(3), 115–133. https://doi.org/10.33176/AACB-19-00024

Yebra, D. M., Kiil, S., & Dam-Johansen, K. (2004). Antifouling technology—past, present and future steps towards efficient and environmentally friendly antifouling coatings. *Progress in Organic Coatings*, *50*(2), 75–104. https://doi.org/10.1016/j.porgcoat.2003.06.001

Yebra, D. M., Kiil, S., Weinell, C. E., & Dam-Johansen, K. (2006). Dissolution rate measurements of sea water soluble pigments for antifouling paints: ZnO. *Progress in Organic Coatings*, *56*(4), 327–337. https://doi.org/10.1016/j.porgcoat.2006.06.007

Ytreberg, E., Bighiu, M. A., Lundgren, L., & Eklund, B. (2016). XRF measurements of tin, copper and zinc in antifouling paints coated on leisure boats. *Environmental Pollution*, *213*, 594–599. https://doi.org/10.1016/j.envpol.2016.03.029

Ytreberg, E., Karlsson, J., & Eklund, B. (2010). Comparison of toxicity and release rates of Cu and Zn from anti-fouling paints leached in natural and artificial brackish seawater. *Science of The Total Environment*, *408*(12), 2459–2466. https://doi.org/10.1016/j.scitotenv.2010.02.036

Ytreberg, E., Lagerström, M., Holmqvist, A., Eklund, B., Elwing, H., Dahlström, M., Dahl, P., & Dahlström, M. (2017). A novel XRF method to measure environmental release of copper and zinc from antifouling paints. *Environmental Pollution*, *225*, 490–496. https://doi.org/10.1016/j.envpol.2017.03.014

Zhang, X., Wang, M., Guo, S., Zhang, Z., & Li, H. (2017). Effects of weathering and rainfall conditions on the release of SiO2, Ag, and TiO2 engineered nanoparticles from paints. *Journal of Nanoparticle Research*, *19*(10), 338. https://doi.org/10.1007/s11051-017-4022-4

Zuin, S., Gaiani, M., Ferrari, A., & Golanski, L. (2014). Leaching of nanoparticles from experimental water-borne paints under laboratory test conditions. *Journal of Nanoparticle Research*, *16*(1), 2185. https://doi.org/10.1007/s11051-013-2185-1

Appendix: Supplementary Information for Chapter 2

Table A1. Composition of MicronCSC-CA antifouling paint, according to the manufacturer.

Ingredient	Weight percentage (%)
Copper (I) oxide	30 - 60
Zinc oxide	10 - 30
Xylene	7 - 13
Iron oxide	3 - 7
Butyl alcohol, n-	3 - 7
Ethyl benzene	1 - 5
Ethyl toluene sulfonamide	1 - 5
Copper (II) oxide	1 - 5

Table A2. Composition of the base Interprotect2000E primer paint, according to the manufacturer.

Ingredient	Weight percentage (%)
Polymer of epoxy resin and bisphenol A	10 - 25
Talc	10 - 25
Barium sulfate	10 - 25
Titanium dioxide	10 - 25
Mica	1.0 - 10
Xylenes	1.0 - 10
Butanol	1.0 - 10
Petroleum naphtha	1.0 - 10
1,2,4-Trimethyl benzene	1.0 - 10
Benzene, ethyl-	1.0 - 10
1,3,5-Trimethylbenzene	1.0 - 10

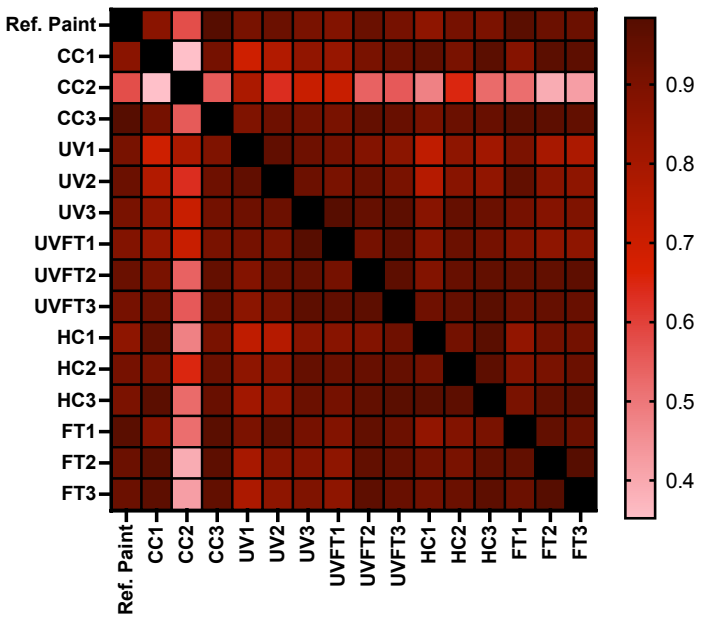

Figure A1. A heatmap of Pearson correlation coefficients comparing paint particles from treatments and reference AF paint (denoted as Ref. Paint). The average of nine spectra were used for each comparison. Treatments are denoted as CC = cold control, HC = heat control, UV = UV irradiation, FT = freeze-thaw, and UV-FT = UV and FT combination. Each replicate is denoted after the treatment name. Black squares indicate the correlation is equal to 1.

CC had the lowest calculated coefficient, which, having experienced the least weathering exposure is surprising. When looking at the CC treatment triplicates individually, CC2 had the lowest Pearson correlation coefficient (Figure A3). The particles used to acquire spectra in this sample were quite small (<50 µm). Interference from the filter may have added unnecessary peaks. Also, insufficient material from the paint particles may have affected the signal intensity (Figure A4). Overall, comparing all the weathered paint particles to each other revealed high correlation coefficients. This confirms that the spectra, even among weathered paints, were very similar, with no observable changes in the organic component of paint.

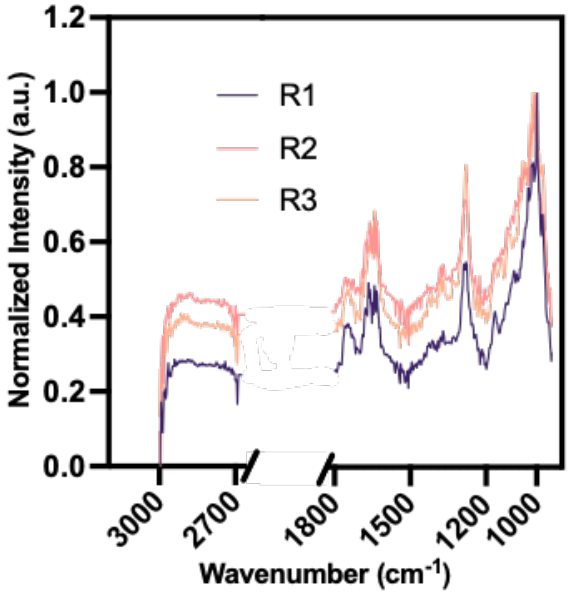

Figure A2. Average of normalized spectra (n = 9) for each replicate procedural filter blank (3000 cm^{-1} to 940 cm^{-1}). R denotes a replicate.

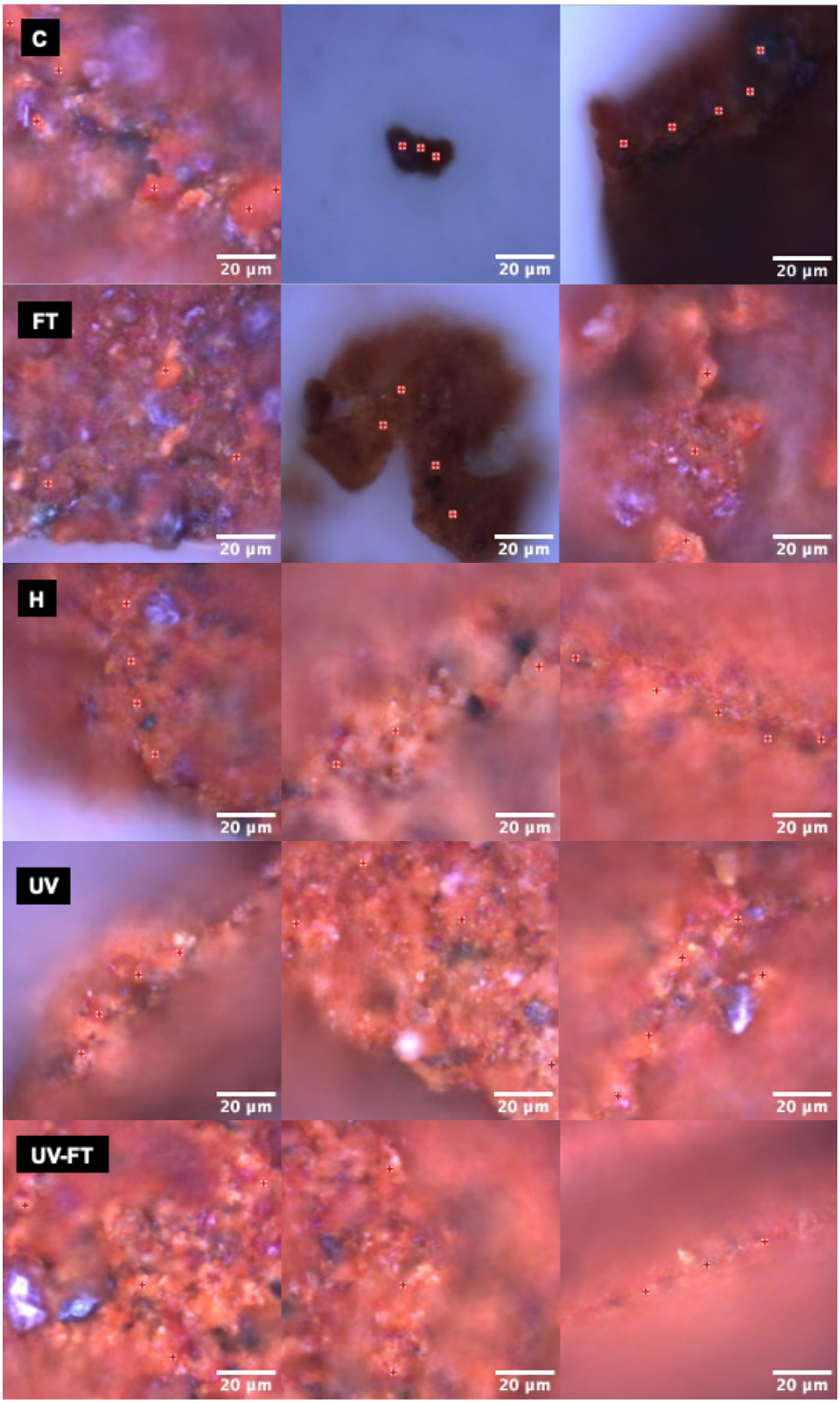

Figure A3. Paint particles of different weathering treatments and controls from which the O-PTIR spectra were acquired. Red markers show spots where a spectrum was acquired.

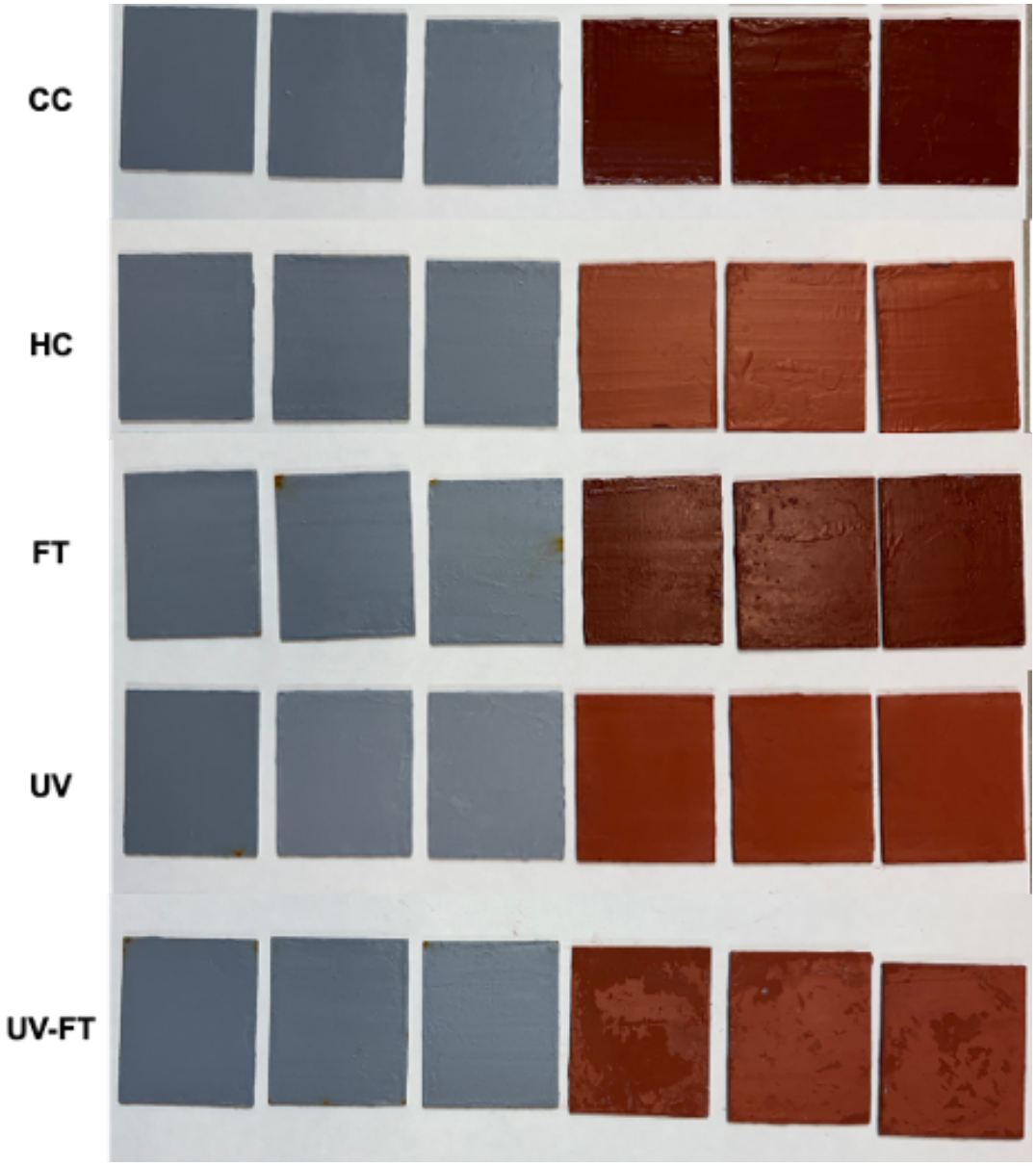

Figure A4. Images of coupons for primer paint (grey coupons) and AF paint (red coupons) after a six-week exposure to the appropriate weathering treatment. Treatments are denoted as CC = cold control, HC = heat control, UV = UV irradiation, FT = freeze-thaw, and UV-FT = UV and FT combination.

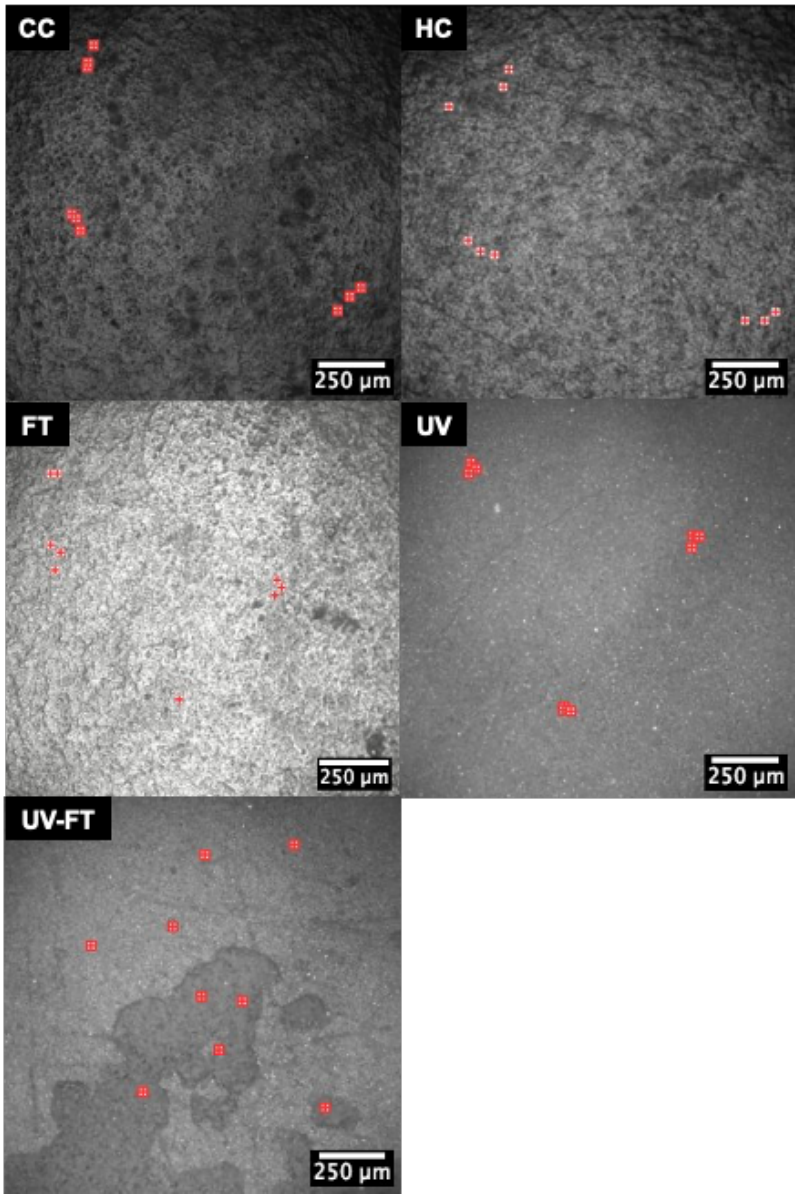

Figure A5. Images of coupons taken with the O-PTIR for AF paint after a six-week exposure to the appropriate weathering treatment. Treatments are denoted as CC = cold control, HC = heat control, UV = UV irradiation, FT = freeze-thaw, and UV-FT = UV and FT combination. Red markers show spots where a spectrum was acquired.

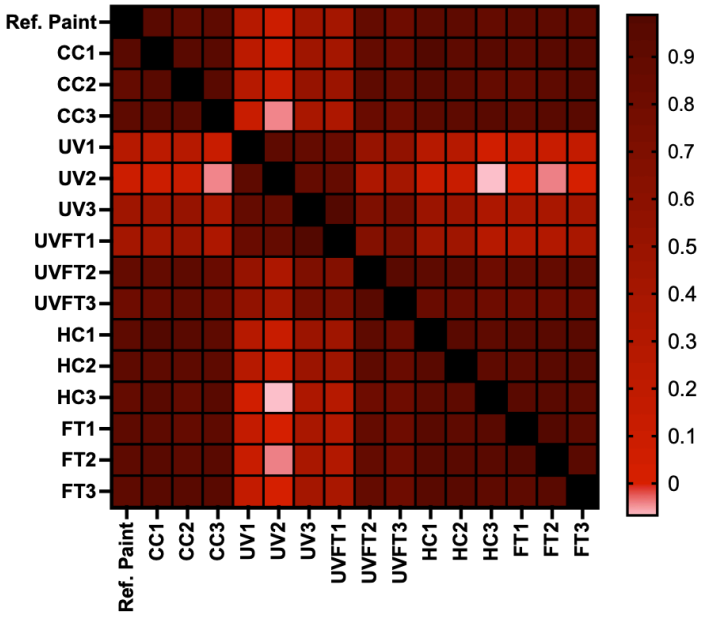

Figure A6. A heatmap of Pearson correlation coefficients comparing exposed paint coupons and reference AF paint (denoted as Ref. Paint). The average of nine spectra were used for each comparison. Treatments are denoted as CC = cold control, HC = heat control, UV = UV irradiation, FT = freeze-thaw, and UV-FT = UV and FT combination. Each replicate is denoted after the treatment name. Black squares indicate the correlation is equal to 1.

Table A3. Average Pearson correlation coefficient (n = 9) of weathered AF paint particles compared to weathered AF paint coupons.

Weathering treatment/control	*CC coupon*	*UV coupon*	*UV-FT coupon*	*HC coupon*	*FT coupon*
CC paint particles	**0.67**	0.35	0.62	0.69	0.69
UV paint particles	0.82	**0.43**	0.74	0.81	0.80
UV-FT paint particles	0.82	0.35	**0.72**	0.84	0.84
HC paint particles	0.73	0.31	0.65	**0.79**	0.80
FT paint particles	0.83	0.13	0.59	0.85	**0.87**

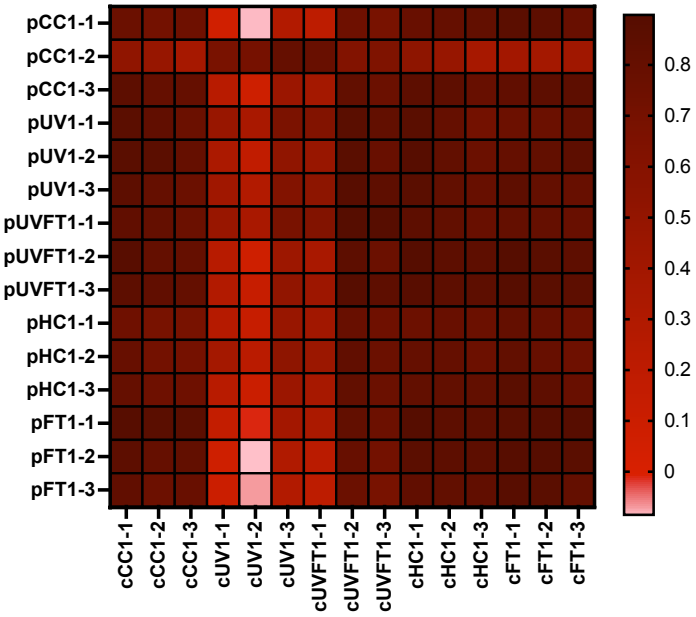

Figure A7. A heatmap of Pearson correlation coefficients comparing weathered paint particles from AF paints and exposed paint coupons of AF paint. The average of nine spectra were used for each comparison. Each comparison is denoted as either p = paint particles and c = coupon. Treatments or controls are denoted as CC = cold control, HC = heat control, UV = UV irradiation, FT = freeze-thaw, and UV-FT = UV and FT combination. Each replicate is denoted after the treatment or control name. Black squares indicate the correlation is equal to 1.

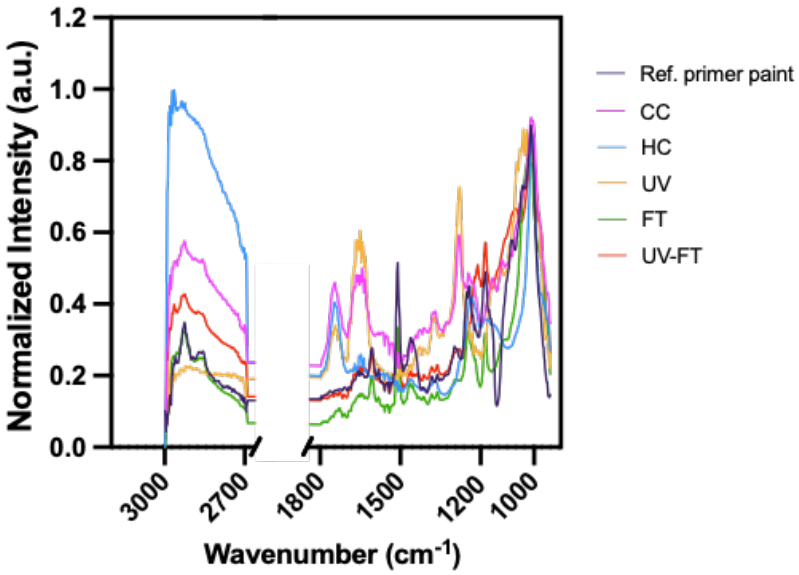

Figure A8. Average of 27 normalized spectra for particles found in triplicate samples of five weathering treatments (i.e., CC = cold control, HC = heat control, UV = UV irradiation, FT = freeze-thaw, and UV-FT = UV and FT combination) compared to the mean from 9 normalized spectra of the virgin reference primer paint, denoted as Ref. Paint. Common wavenumbers shared among all spectra are labelled (3000 cm^{-1} to 940 cm^{-1}).

Table A4. Descriptive statistics of particle sizes and particle counts of microscopic images from weathered AF paint treatments, analyzed using ImageJ. All values were blank subtracted.

Weathering treatment/control	Median size (mm ± SD)	Mean size (mm ± SD)	Maximum size (mm ± SD)	Minimum size (mm ± SD)	Mean particle count (particles/mL ± SD)
Control (CC)	0.03 ± 0.01	0.04 ± 0.007	0.7 ± 0.5	0.007 ± 0.0002	2 ± 3
Heat Control (HC)	0.02 ± 0.00	0.04 ± 0.02	1.1 ± 0.7	0.007 ± 0.0002	6 ± 6
Freeze-Thaw (FT)	0.03 ± 0.01	0.07 ± 0.02	3.3 ± 1.0	0.006 ± 1E-18	67 ± 30
UV	0.02 ± 0.00	0.03 ± 0.004	1.0 ± 0.3	0.006 ± 0.0006	14 ± 10
UV-FT*	0.08 ± 0.05	0.20 ± 0.10	4.8 ± 0.1	0.006 ± 0.0006	10 ± 10

*Particle counts and size for UV-FT were not accurately representative due to the saturation of the filter with paint particles.

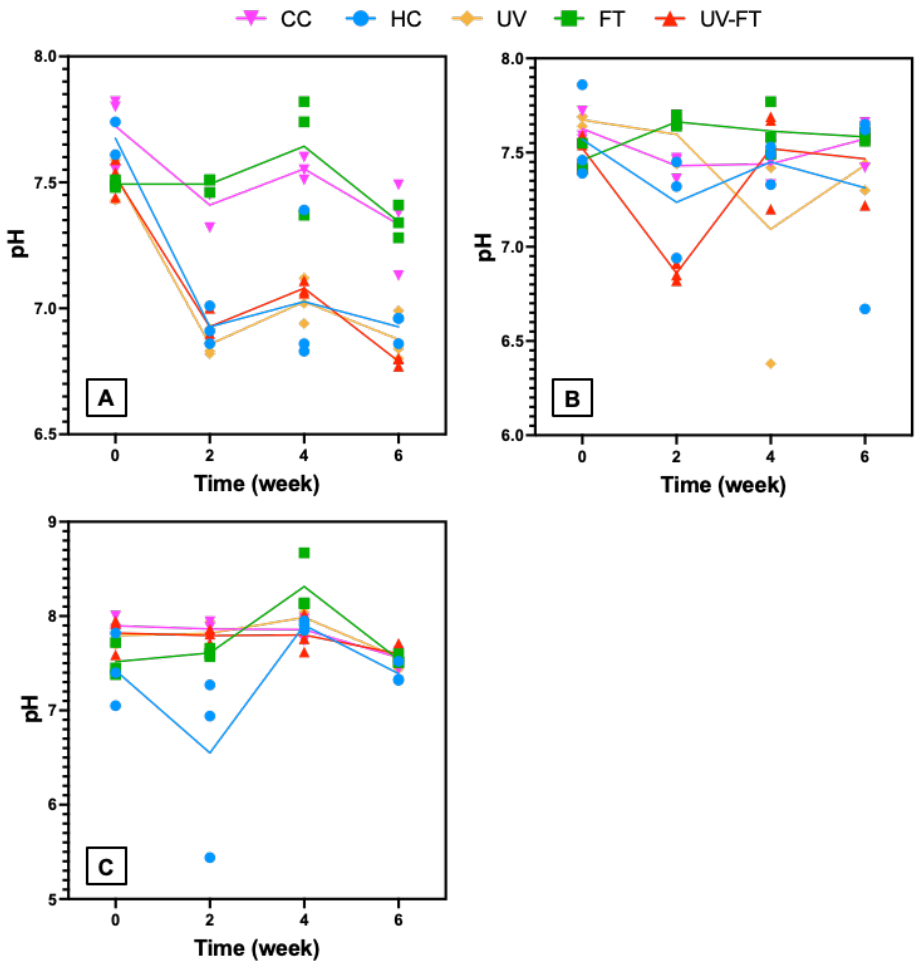

Figure A9. pH measurements for (A) AF paint; (B) primer paint; and (C) procedural blanks exposed to the appropriate weathering treatment. The connected lines at each timepoint represent the median. Each replicate measurement is shown for every timepoint (n = 3).

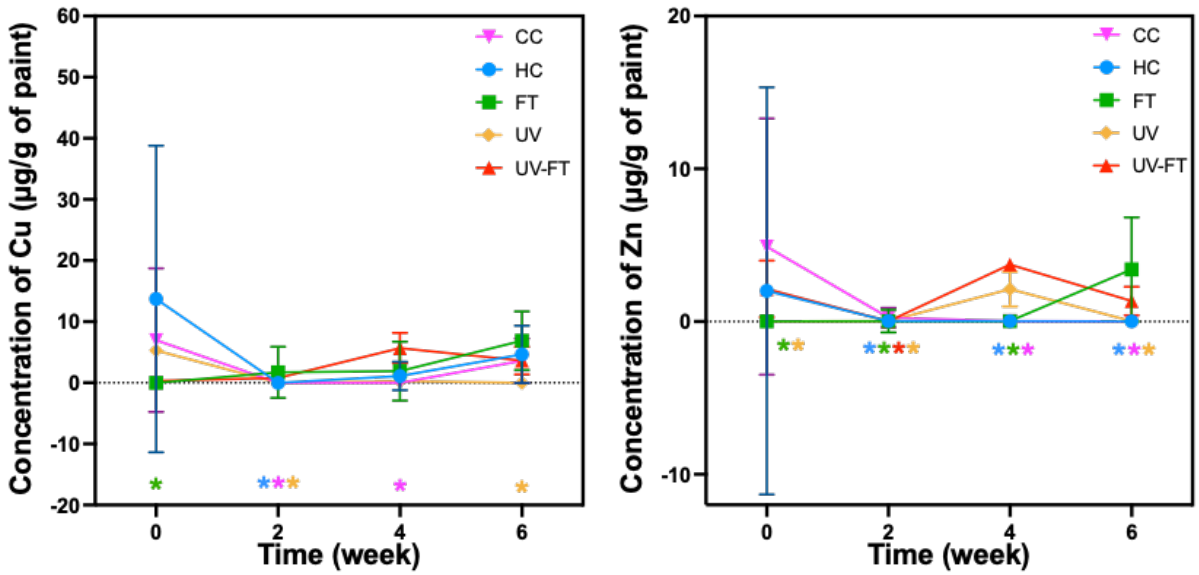

Figure A10. Release from primer paint of average total Cu (left) and Zn (right), denoted in µg/g of dry paint, from five weathering treatments in F2. Error bars denote the standard deviation around the mean. Asterisks with their appropriate treatment denote values that are below the limit of detection and are equal to LOD/2.

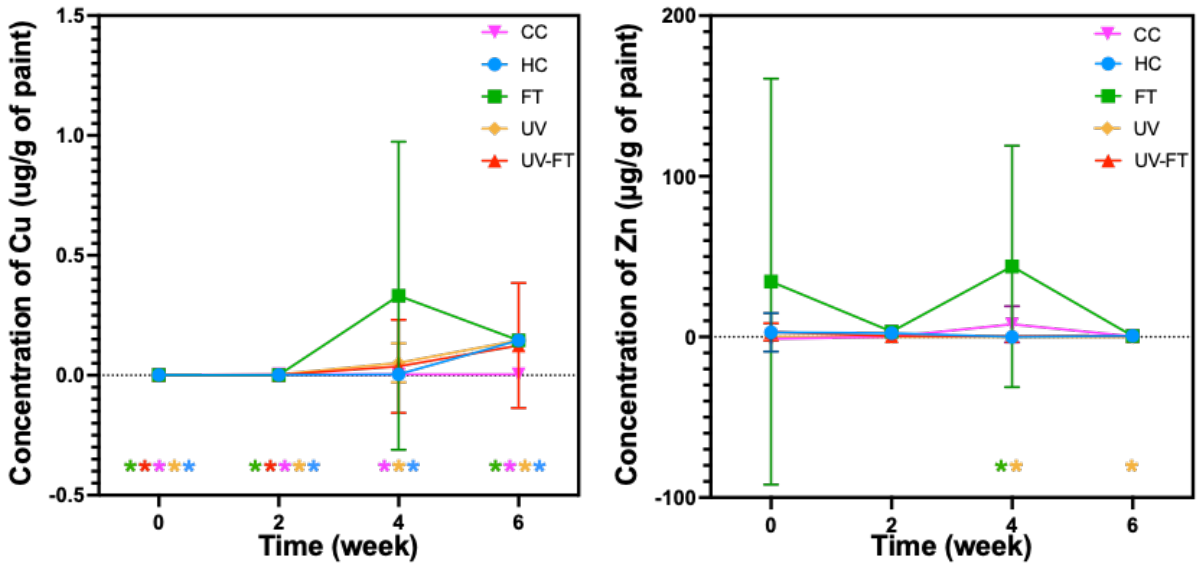

Figure A11. Release from primer paint of average total Cu (left) and Zn (right), denoted in µg/g of dry paint, from five weathering treatments in F3. Error bars denote the standard deviation around the mean. Asterisks with their appropriate treatment denote values that are below the limit of detection and are equal to LOD/2.

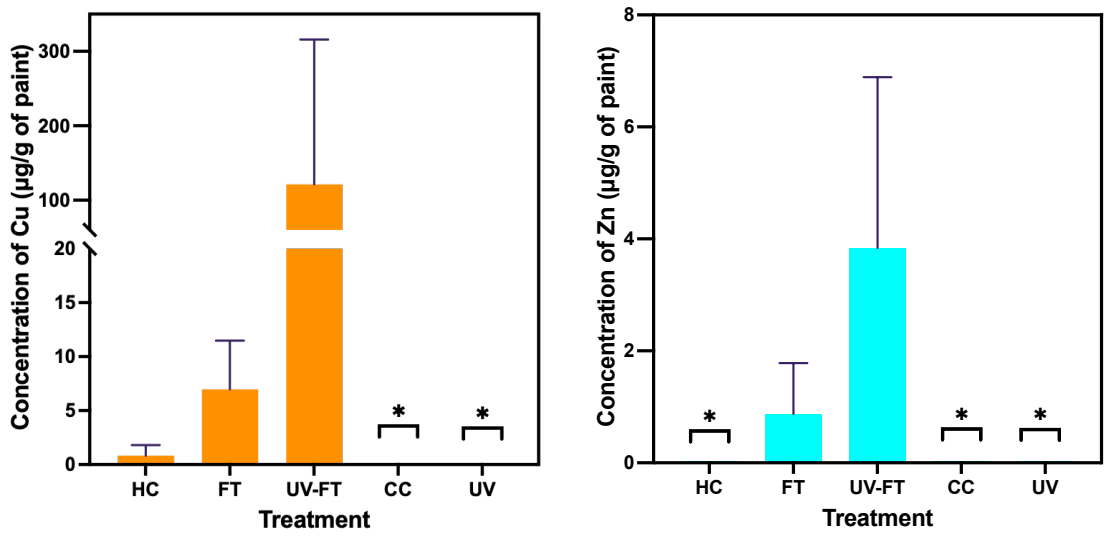

Figure A12. Concentrations, denoted in µg/g of dry paint, of Cu (left) and Zn (right) in five weathering treatments in F1 for primer paint. Error bars denote the standard deviation around the mean. Asterisks denote values that are below the limit of detection and are equal to LOD/2.

Table A5. Nanoparticle tracking measurements for AF paint exposed to five different treatments, measured in number of particles per mL. All values were blank subtracted.

Weathering treatment/control	Timepoint (weeks)	Measurement (# of particles/mL)		
Control (CC)	0	N.d.	N.d.	N.d.
	2	2.9E+7	1.5E+7	N.a.
	4	4.4E+7	N.d.	3.0E+7
	6	2.6E+7	N.d.	N.d.
Heat Control (HC)	0	1.1E+8	1.6E+8	3.9E+7
	2	7.1E+7	N.d.	N.d.
	4	1.1E+8	N.d.	N.a.
	6	3.0E+6	N.d.	N.a.
Freeze-Thaw (FT)	0	N.d.	N.a.	1.3E+8
	2	N.d.	N.a.	N.a.
	4	N.a.	N.a.	8.0E+6
	6	N.a.	N.a.	7.1E+7
UV	0	2.2E+7	1.8E+7	2.7E+7
	2	N.d.	5.8E+6	4.7E+7
	4	1.1E+7	8.3E+7	1.1E+8
	6	4.8E+7	N.a.	3.5E+7
UV-FT	0	3.1E+8	6.2E+7	1.0E+8
	2	3.4E+7	3.4E+7	3.4E+7
	4	1.4E+8	1.4E+8	1.4E+8
	6	2.9E+8	N.a.	1.5E+7

N.d.: not detected, below the limit of detection (<100 valid tracks); N.a.: not applicable, tracks were valid but negative value after blank subtraction.

At timepoint 0 weeks, nanosized particles were detected in all treatments of AF paint, except for CC. The painted coupons were washed with demineralized water before immersion in the jar, to ensure that loose particles from the paint or other miscellaneous particles (such as dust) were removed and not included in the analysis. Clearly, this could not be avoided. These initial particles seem to have settled out after 2 weeks, with lower particle number concentrations measured after said timepoint (Table A4). After the 6-week timepoint, particle number concentrations for AF paint were lower in the UV and HC treatments, but slightly higher for UV-FT, FT and CC conditions compared to the 2-week timepoint. Results suggest that most particles generated from paint binder were in the micro-range.

Table A6. Nanoparticle tracking measurements for primer paint exposed to five different treatments, measured in number of particles per mL. All values were blank subtracted.

Weathering treatment/control	Timepoint (weeks)	Measurement (# of particles/mL)		
Control (CC)	0	N.d.	N.d.	N.d.
	2	1.5E+7	N.d.	1.1E+7
	4	N.a.	N.d.	N.a.
	6	1.0E+7	7.8E+6	1.5E+8
Heat Control (HC)	0	2.4E+8	4.9E+7	7.0E+7
	2	6.0E+8	2.9E+8	3.5E+7
	4	7.0E+7	1.3E+7	2.3E+7
	6	3.5E+7	N.a.	2.6E+7
Freeze-Thaw (FT)	0	N.a.	N.a.	N.a.
	2	9.9E+6	7.3E+7	2.9E+8
	4	2.3E+8	2.4E+8	N.a.
	6	2.2E+8	6.0E+7	5.2E+6
UV	0	N.d.	3.9E+7	N.d.
	2	2.7E+7	4.2E+7	8.0E+7
	4	N.d.	N.d.	8.2E+7
	6	2.9E+6	4.1E+7	5.3E+6
UV-FT	0	3.3E+8	3.9E+7	5.1E+8
	2	1.2E+8	1.5E+8	N.d.
	4	10.0E+7	7.2E+7	8.0E+7
	6	4.3E+7	N.d.	N.a.

N.d.: not detected, below the limit of detection (<100 valid tracks); N.a.: not applicable, tracks were valid but negative value after blank subtraction.

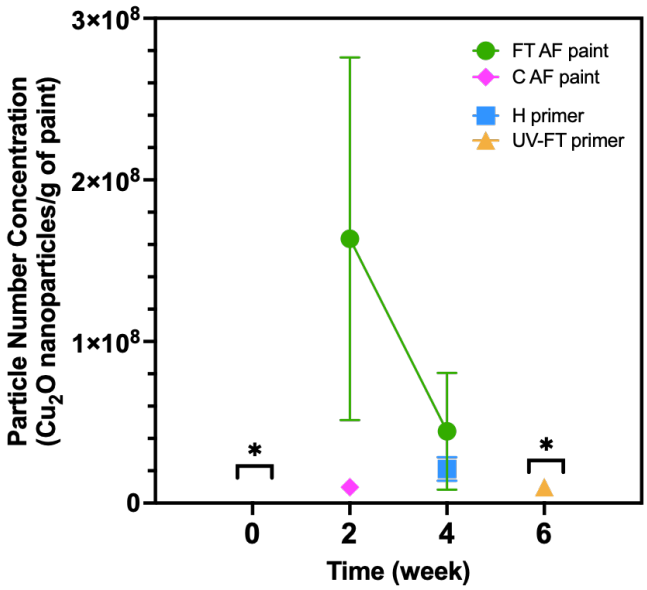

Figure A13. Average number concentrations of Cu_2O nanoparticles per gram of dry paint (number of nanoparticles/g of dry paint). Concentrations are shown for AF paints exposed to FT and CC treatments, and primer exposed to UV-FT and HC treatments as a function time (weeks). Error bars denote standard deviation of triplicate measurements (n = 3). Asterisks denote time points that were below the limit of detection (<200 particle events).

The number of nanoparticles released from the primer were lower than those released from the AF paint (Figure A10). Since Cu was not listed as a component in the material safety data sheet of the primer paint, these particles may be present as impurities in the talc or the mica (listed components in the basecoat, Table A2), resulting in their subsequent release.

Table A7. Average mass concentration (ppb ± SD), average dissolved (ionic) background (ppb ± SD), and fraction of average mass concentration of Cu_2O divided by the average dissolved background (% ± SD) obtained from untreated SP-ICP-MS data. Individual triplicates are shown for the relevant weathering treatments.

Weathering treatment/control	Average median size (mm ± SD)	Average mean size (mm ± SD)	Average maximum size (mm ± SD)	Average minimum size (mm ± SD)	Average mean particle count (particles/mL ± SD)
Control (CC)	0.03 ± 0.01	0.040 ± 0.007	0.7 ± 0.5	0.0070 ± 0.0002	2 ± 3
Heat Control (HC)	0.02 ± 0.00	0.04 ± 0.02	1.1 ± 0.7	0.0070 ± 0.0002	6 ± 6
Freeze-Thaw (FT)	0.03 ± 0.01	0.07 ± 0.02	3.3 ± 1.0	0.006 ± 1E-18	67 ± 30
UV	0.02 ± 0.00	0.030 ± 0.004	1.0 ± 0.3	0.0070 ± 0.0006	14 ± 10
UV-FT*	0.08 ± 0.05	0.2 ± 0.1	4.8 ± 0.1	0.0060 ± 0.0006	10 ± 10

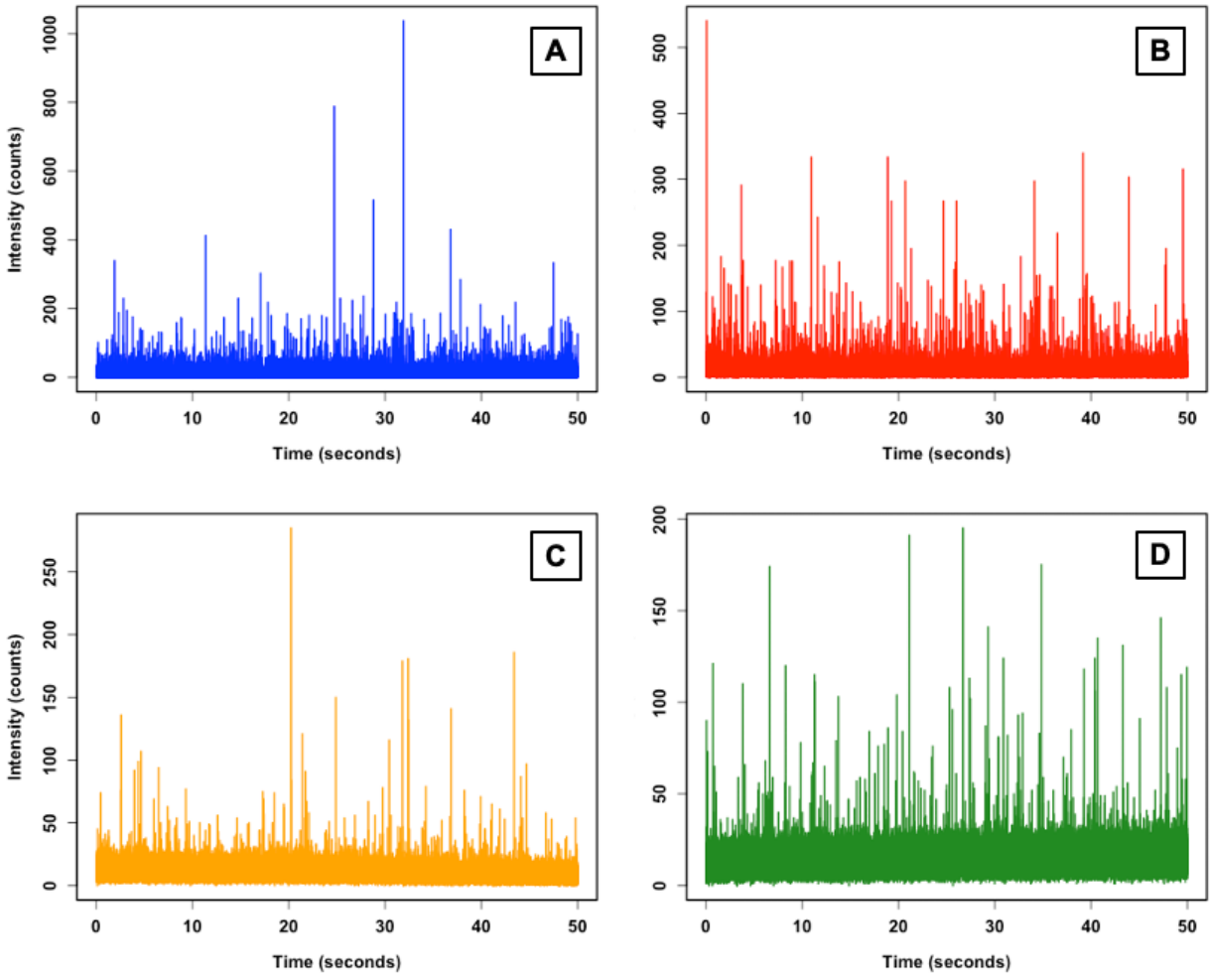

Figure A14. Examples of raw SP-ICP-MS data for Cu_2O released from AF paints exposed to (A) FT treatment at 2 weeks, (B) FT treatment at 4 weeks, (C) FT treatment at 6 weeks, and (D) CC control at 2 weeks.

Table A8. Weight of paint (antifouling paint + primer paint) applied to coupons exposed to different weathering treatments. The weights shown are for the AF paint.

Weathering treatment	Weight of paint before weathering (g)	Weight of paint after weathering (g)	Weight of paint lost (g)
Control (CC)	4.389	4.375	0.014
	4.468	4.454	0.015
	4.202	4.188	0.015
Heat Control (HC)	4.151	4.019	0.132
	4.274	4.141	0.133
	4.477	4.336	0.142
Freeze-Thaw (FT)	4.533	4.481	0.052
	4.681	4.644	0.037
	4.482	4.376	0.106
UV	4.319	4.173	0.146
	4.382	4.233	0.149
	4.339	4.193	0.146
UV-FT	3.957	3.529	0.429
	4.386	3.939	0.447
	4.994	4.401	0.593

Table A9. Weight of paint (primer paint only) applied to coupons exposed to different weathering treatments. The weights shown are for the primer paint. Weights after weathering may be higher due to formation of rust.

Weathering treatment	Weight of paint before weathering (g)	Weight of paint after weathering (g)	Weight of paint lost (g)
Control (CC)	3.154	3.065	0.089
	3.248	3.152	0.096
	1.595	1.418	0.177
Heat Control (HC)	2.419	1.681	0.738
	2.569	2.150	0.420
	2.290	2.117	0.174
Freeze-Thaw (FT)	1.868	3.102	N.a.
	2.151	2.617	N.a.
	2.188	2.159	N.a.
UV	3.114	2.985	0.129
	3.429	3.300	0.129
	1.489	3.733	N.a.
UV-FT	2.613	1.495	1.118
	2.896	2.842	0.055
	2.618	2.570	0.048

N.a.: not applicable.

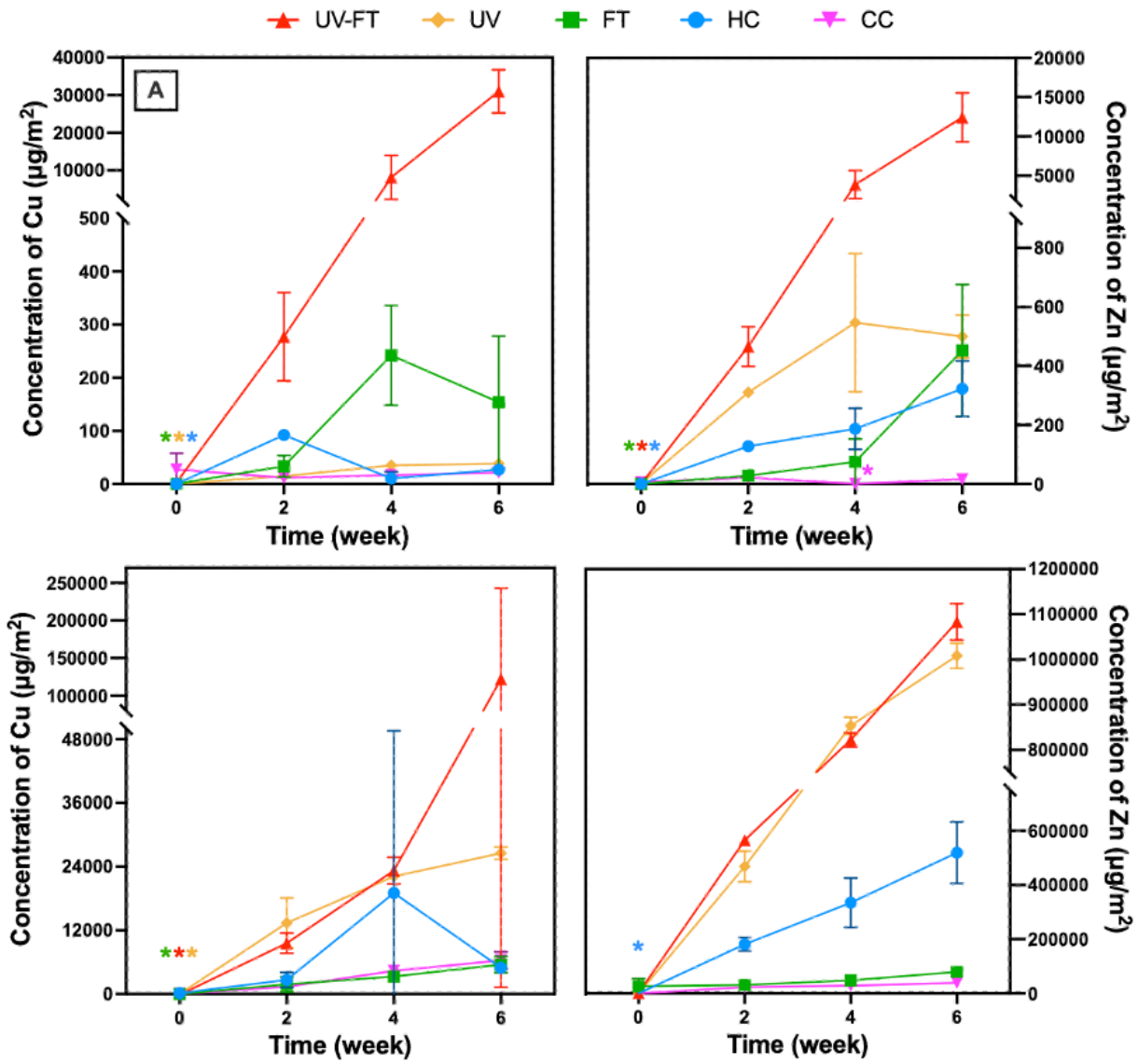

Figure A15. Blank subtracted average total Cu (left) and Zn (right) concentrations released from AF paint, in µg/m^2, from five weathering treatments in the F2 (A and B) and F3 (C and D). Concentrations were normalized to coupon area. Error bars denote the standard deviation around the mean of triplicate samples. Asterisks with their appropriate treatment denote values that are below the limit of detection and are equal to LOD/2.